Design and experimental study of a hybrid vibration absorber for global vibration control

M.H. Tso, J. Yuan, W.O. Wong

Department of Mechanical Engineering, The Hong Kong Polytechnic University, Hong Kong

ABSTRACT

A simple and practical hybrid vibration absorber (HVA) is proposed for global vibration control of flexible structures under random stationary excitations. The HVA, regulated by a pole placement controller, uses a linear translational feedback signal to synthesize active moment via a moment actuator. It is shown, analytically and experimentally, capable of damping vibration in the entire primary structure. While the passive tuned mass damper (TMD) can suppress tonal vibration in the primary structure at the vicinity of the coupling point, it enhances vibration at other locations and other frequencies. The presented HVA, in contrast, can provide more than 48% extra broadband attenuation on vibrations at multiple points when compared with the passive TMD in experimental verification on a beam structure. Up to 85% extra broadband attenuation can be observed at the coupling point. The proposed HVA is a simple and economic alternative for engineers to retrofit the conventional TMD to a higher performance HVA for damping vibrations at multiple locations of the primary structure.

Keywords: System identification, Global vibration control, Vibration absorber, Hybrid control

1. INTRODUCTION

The viscous damper is a well-known, effective and economic device for attenuating vibrations in structures like frames [1, 2] and bridges [3-6]. Practically, a viscous damper may be mounted between two vibrating structures in order to damp relative motion [1-6]. It is also possible to mount a viscous damper between a vibrating structure and a relatively “fixed” base such as ceiling or ground to be a "hooked damper" [7, 8]. No matter which mounting method is used, a viscous damper needs a backed-up point at one end. This restriction may limit the applicability of viscous dampers in some mechanical structures with free-end boundaries, or some applications where it is impossible to find nearby rigid supports.

The tuned mass dampers (TMD), on the other hand, are widely used for structural vibration control [9-13]. Figure 1 shows a TMD for vibration control in many skyscrapers, such as the "Taipei 101". It only requires a point of attachment instead of a point of rigid support. The vibration of the primary structure will cause the suspended mass to swing. As a result, tensions in the suspension

cables are different, creating coupling moment and force to counteract the structural vibration [15]. A TMD is extremely effective attenuating vibration in a narrow frequency range in the vicinity of the mounting position. It could, however, develop some negative effect at points far away from the coupling location [16] or enhance vibration in other frequencies. If one increases damping ratio of a TMD to avoid enhancing vibration in other frequencies, the attenuation dip will be deteriorated since a TMD requires weak damping to suppress narrow-frequency vibration of the primary structure. Some researchers propose to find optimal damping ratio for the TMD based on accurate knowledge of eigen-functions, resonant frequencies and modal damping ratios of the primary structure. After choosing the optimal damping ratio for a TMD, how to implement it accurately is another practical problem.

The above problems of the TMD may be solved by integrating an active element into a conventional TMD. One may retrofit a TMD to a hybrid vibration absorber (HVA) with better performance for broadband vibration control [17, 18]. Recent advances in the designs of HVA can be found in the literature [17, 23]. Most available active controllers focus on suppressing vibration at a single point. A simple HVA is proposed by the authors for broadband vibration control over multiple points in a primary structure [23].

In the literature, most researchers assume accurate knowledge of eigen-functions and eigen-state feedback of the primary structures for controller design, implementation and stability analysis. In real applications, eigen-functions and eigen-states of primary structures are usually not available with sufficient accuracy. Active controller design may be based on identified models like discrete-time transfer functions. The design and stability analysis of controllers will be different due to different models and mathematical tools. This problem is addressed here. A simple active controller is designed and implemented based on a TMD similar to the one shown in Fig. 1. The new system only uses a linear accelerometer and a moment actuator to form a practical and economic HVA for structural vibration control. The proposed HVA is able to damp global broadband vibration in primary structures. Experimental data are presented to demonstrate the excellent global control performance.

2. THEORY

The HVA presented here is simpler than its previous version [23] in the feedback sensor. A single-axis translational accelerometer, which is easily available and easy to install, is used instead of an angular displacement sensor. While it is possible to measure angular displacement with a piezoelectric sensor, the signal is proportional to the averaged bending over sensor length instead of

angular displacement at a point. If the sensor length is not significantly smaller than the dimension of the primary structure, then spatial average effects of a piezoelectric sensor cannot be approximated accurately by a spatial Dirac delta function as assumed by many researchers in the literature. This is a problem in our experiments with a scaled primary structure, or other applications with small size primary structures. The translational accelerometer, on the other hand, is economic and smaller than the scaled primary structure in our experiments or other similar applications. The seemingly trivial sensor replacement causes some non-trivial changes of model properties, which could affect the controller design. The "unusual" combination of a translational feedback sensor with a moment actuator can be an alternative to some applications where the "usual" combination of translational sensors with force actuators or angular sensors with moment actuators could not be adopted due to some possible unforeseeable difficulties. It is explored in this study in details to show that the proposed HVA is independent of combinations of feedback sensors with actuators. The proposed HVA also differs from available counterparts since its parameters do not depend on accurate knowledge of eigen-functions of the primary structure and the controller does not require eigen-state feedback. This is a significant feature since eigen-functions and eigen-states of the primary structure are not available with sufficient accuracy in most practical applications. Even if eigen-functions of the primary structure are available accurately, eigen-state feedback requires multichannel feedback signals measured at multiple points of the primary structure. For ease of practical implementation, the proposed HVA parameters depend on the identified transfer function and a single feedback signal. Structural vibration response is monitored in experimental study in terms of mean square velocity and power spectral density (PSD) to evaluate the performance of the active controller on global vibration control. Some theoretical issues relating to the difference in mathematical model, the design and analysis tool are clarified here and in Section 3.2 respectively.

A cantilever beam, shown in Fig. 2, is used as the primary structure for theoretical study and experimental verification. The angular, linear displacements and velocity of the beam are denoted as $\theta(x,t)$, $w(x,t)$ and $v(x,t)$ respectively. The HVA is coupled with the beam at $x = x_a$ in Fig. 2. The angular displacement of the suspended mass is denoted as $\phi(t)$. A coupling moment generated by the HVA is denoted as $\tau(t)$. Its effect on the beam is described by $\tau(t)\delta(x - x_a)$, where $\delta(x - x_a)$ is a spatial Dirac delta function. The external disturbance is modeled by a moment function excited at $x = x_d$ and denoted as $r(t)\delta(x - x_d)$, where $r(t)$ is a stationary and random time function. Damping and displacement of the beam satisfy the Kelvin-Voigt [24] and Euler-Bernoulli hypothesis respectively. The dynamic equations of the coupled system can be written as

$$\rho\ddot{w}(x,t)+CI\dot{w}''''(x,t)+EIw''''(x,t)=\frac{\partial[r(t)\delta(x-x_d)]}{\partial x}+\frac{\partial[\tau(t)\,\delta(x-x_a)]}{\partial x},\quad 0<x<L \tag{1}$$

$$\tau(t)=k[\phi(t)-\theta_a(t)]+m_{\text{act}}(t) \tag{2}$$

$$\tau(t)=-J\,\ddot{\phi}(t) \tag{3}$$

In Eq. (1), ρ, C, E and I represent, respectively, mass per unit length, damping coefficient, Young's modulus and second moment of cross sectional area of the beam. Equation (2) models the temporal effects of the coupling moment $\tau(t)$, with the active component $m_{act}(t)$ generated by a moment actuator. Effect of the rotational spring is modeled by stiffness k. Equation (3) relates the coupling moment $\tau(t)$ with the angular acceleration $\ddot{\phi}(t)$ and the second moment of inertia J of the HVA. In modal space, the linear displacement of the beam can be represented as

$$w(x,t)=\sum_{i=1}^{\infty}\eta_i(t)\varphi_i(x), \tag{4a}$$

The linear velocity of the beam can be expressed as

$$v(x,t)=\dot{w}(x,t)=\sum_{i=1}^{\infty}\dot{\eta}_i(t)\varphi_i(x), \tag{4b}$$

The angular displacement of the beam can be written as

$$\theta(x,t)=-\frac{\partial w(x,t)}{\partial x}=-\sum_{i=1}^{\infty}\eta_i(t)\varphi_i'(x). \tag{4c}$$

where $\eta_i(t)$ and $\dot{\eta}_i(t)$ are the ith modal eigen-state and its derivative with respect to time; $\varphi_i(x)$ and $\varphi_i'(x)$ are the ith modal eigen-function of the beam and its derivative with respect to x.

A translational velocity signal is used as the feedback, and the active moment is synthesized with a control law, whose Laplace transform domain version is

$$M_{act}(s)=G(s)V_a(s) \tag{5}$$

where $M_{act}(s)=\mathcal{L}[m_{act}(t)]$, $V_a(s)=V(x_a,s)=sW(x_a,s)=\mathcal{L}[\,\dot{w}(x_a,t)\,]$ and $G(s)$ is the controller transfer function to be discussed in Section 3.2. Let $\frac{V(x,s)}{R(s)}$ denotes the closed-loop transfer function from the disturbance to any location x in the primary system, then $\frac{V(x,s)}{R(s)}$ is derived in Appendix A as:

$$\frac{V(x,s)}{R(s)} = \frac{-sK(s)B_{xd'}(s) + s^3 k\Delta B_k(s) + s^4 G(s)\Delta B_G(s)}{A(s)K(s) + s^2 kB_{a'a'}(s) + s^3 G(s)B_{aa'}(s)} \tag{6}$$

Detailed definitions of $B_{xd'}(s)$, $\Delta B_k(s)$, $\Delta B_G(s)$, $B_{a'a'}(s)$ and $B_{aa'}(s)$ are given in Appendix A.

In Eq. (6), the denominator (characteristic equation) of the closed-loop transfer function is independent of spatial variable *x* under active control. This means active global damping is possible with the proposed HVA by a proper selection of *G*(*s*). The damping effects apply to all points of entire primary structure instead of at the coupling point. The use of translational accelerometer causes a small change in Eq. (6): the characteristic equation changes from $A(s)K(s) + s^2 kB_{a'a'}(s) + s^2 G(s)B_{a'a'}(s)$ in [23] to $A(s)K(s) + s^2 kB_{a'a'}(s) + s^3 G(s)B_{aa'}(s)$ here. Due to the difference between $s^2 B_{a'a'}(s)$ and $s^3 B_{aa'}(s)$, the secondary path transfer function becomes possibly non minimum phase. This is a practical problem since spatial effects of actuators may not necessarily be represented by spatial Dirac delta functions accurately. Even with a collocated translational sensor and force actuator combination, the secondary path transfer function could still be non minimum phase when the implementation is a discrete-time system. It could affect some controllers, such as the direct velocity feedback controllers that become unstable to non minimum secondary control paths. The proposed HVA, however, is independent of such a difference and independent of different combinations of feedback sensors with actuators and their respective locations.

The proposed HVA also differs from other available counterparts since its parameters do not depend on eigen-functions of the primary system and it does not use eigen-state feedback. Instead, the controller parameters depend on a discrete-time transfer function

$$\frac{V(x,z)}{R(z)} = \frac{-K(z)B_{xd'}(z) + k\Delta B_k(z) + G(z)\Delta B_G(z)}{A(z)K(z) + kB_{a'a'}(z) + G(z)B_{aa'}(z)} \tag{7}$$

where $B_{xd'}(z)$, $\Delta B_k(z)$, $\Delta B_G(z)$, $B_{a'a'}(z)$ and $B_{aa'}(z)$ are mathematically related to $B_{xd'}(s)$, $\Delta B_k(s)$, $\Delta B_G(s)$, $B_{a'a'}(s)$ and $B_{aa'}(s)$. Practically, parameters of the proposed controller only depend on polynomials $Q(z) = A(z)K(z) + kB_{a'a'}(z)$ and $B_{aa'}(z)$, which can be identified with sufficient accuracy.

3. DESIGN OF THE HVA

This section will mainly discuss on the hardware and controller design of the HVA.

3.1 HARDWARE DESIGN

The rotational tuned mass damper in Fig. 1 is widely used in buildings or skyscrapers for structural vibration control [19]. It generates moment and horizontal force at the anchor position by the suspended cables when the primary structure vibrates. Figure 3 briefly shows how the moment is generated by the suspended cable. Let *T1* and *T2* denote tensions in the suspended cables when the suspended mass swings. The tensions may be expressed, respectively, as $F1_{vertical}$, $F1_{horizontal}$, $F2_{vertical}$ and $F2_{horizontal}$. Since tensions *T1* and *T2* are different in magnitudes when the mass swings, $F1_{vertical}$ and $F2_{vertical}$ are also different in magnitudes to generate dynamic moment acting on the top center position of the primary structure.

Conventionally, the pendulum type tuned mass damper shown in Fig. 1 can be retrofitted to a hybrid vibration absorber by integrating a translational *x*-*y* table, driven by a set of ball screw and AC servo motor [19]. Figure 4 shows the schematic of such kind of hybrid vibration absorber. The drawback of this design is space occupation of the translational platform. In case of severe vibrations, deformations in the guiding rails could hinder the movement of the suspended mass and deteriorate control performance.

An alternative design of HVA is presented here to tackle the existing problem. Typically, a pendulum type tuned mass damper consists of suspended cables and mass. For vibration at very low frequency, length of suspended cables should be very long to limit its applicability in real practice as very large space is required for absorber installation [25]. The proposed HVA shown in Fig. 5 consists of a flexible connecting beam with a mass and a moment actuator. The mass can be vertically aligned along the center slot of the connecting beam for easy tuning of passive resonant frequency. The other end of the connecting beam is fixed on the primary structure. The moment actuator is adhered to the suspension frame to generate active moment. During vibration control, the HVA mass will swing and bend the connecting beam to generate the passive moment. The coupling moment can be transmitted to the primary structure through the coupling point of the HVA. This design can reduce space consumption due to the long suspended cable and bulky active moving table. It is free of negative effects caused by possible deformation of guiding rails. Alternatively, one may mount actuators parallel to the dampers in the rotational inertia damper of [26] to turn the passive rotational TMD into a HVA.

3.2 CONTROLLER DESIGN

This part provides details on the pole placement controller $G(z)$. The control objective is to introduce damping effect to the poles of the closed-loop system. A prototyped polynomial with selected roots is assigned as the denominator of the closed-loop system. When the active controller is switched off, i.e. $G(z)=0$, the dynamic response of the proposed HVA will automatically turn to a conventional passive absorber (TMD). The active controller has a transfer function

$$G(z) = \frac{P(z)}{U(z)} \tag{8}$$

where $P(z) = \sum_{i=0}^{n-1} p_i z^{-i}$, $U(z) = 1 + \sum_{i=1}^{n-1} u_i z^{-i}$ and n is the order of the secondary path transfer function available by offline system identification [27]. Details of offline system identification will be discussed in the next section. Substituting Eq. (8) into Eq. (7), one obtains the closed-loop transfer function from the disturbance to any location of the HVA coupled system. The result is

$$\begin{aligned} \frac{V(x,z)}{R(z)} &= \frac{[-K(z)B_{xd'}(z) + k\Delta B_k(z)]U(z) + P(z)\Delta B_G(z)}{[A(z)K(z) + kB_{a'a'}(z)]U(z) + P(z)B_{aa'}(z)} \\ &= \frac{[-K(z)B_{xd'}(z) + k\Delta B_k(z)]U(z) + P(z)\Delta B_G(z)}{Q(z)U(z) + P(z)B_{aa'}(z)} \end{aligned} \tag{9}$$

where $Q(z) = A(z)K(z) + kB_{a'a'}(z)$. In Eq. (9), parameter polynomials $P(z)$ and $U(z)$ of the controller contribute to both denominator and numerator of the closed-loop transfer function. Although the denominator is independent on spatial variable x, the closed-loop transfer function is a function of x since polynomials $B_{xd'}(z)$, $\Delta B_k(z)$ and $\Delta B_G(z)$ depend on spatial variable x (proven in Appendix A). It is possible to focus on a single monitor point x and try to reduce either the H_∞ or H_2 norm of Eq. (9) by selecting a proper controller. That is a common approach adopted by most researchers in the literature. The proposed controller, however, is designed to reduce the H_2 norm of Eq. (9) at multiple points instead of just one point. This is another significant feature of the proposed HVA.

Since the denominator of Eq. (9) is independent of spatial variable x, it is the starting point for controller design. By matching the denominator of Eq. (9) to a prototype polynomial $D(z)$, one obtains a Bezout equation

$$Q(z)U(z) + P(z)B_{aa'}(z) = D(z) \tag{10}$$

where $Q(z) = 1 + \sum_{i=1}^{n} q_i z^{-i}$, $B_{aa'}(z) = \sum_{i=0}^{n-1} b_i z^{-i}$ and $D(z) = 1 + \sum_{i=1}^{2n-1} d_i z^{-i}$. The matrix-vector version of Eq. (10) is

$$\begin{pmatrix} 1 & & & & & & & & & & \\ q_1 & 1 & & & & b_0 & & & & & \\ q_2 & q_1 & \ddots & & & b_1 & b_0 & & & & \\ \vdots & q_2 & \ddots & \ddots & & \vdots & b_1 & \ddots & & & \\ \vdots & \vdots & \ddots & \ddots & 1 & \vdots & \vdots & \ddots & \ddots & & \\ q_n & \vdots & \ddots & \ddots & q_1 & b_{n-1} & \vdots & \ddots & \ddots & b_0 & \\ & q_n & \ddots & \ddots & q_2 & & b_{n-1} & \ddots & \ddots & b_1 & \\ & & \ddots & \ddots & \vdots & & & \ddots & \ddots & \vdots & \\ & & & \ddots & \vdots & & & & \ddots & \vdots & \\ & & & & q_n & & & & & b_{n-1} & \end{pmatrix} \begin{pmatrix} 1 \\ u_1 \\ \vdots \\ \vdots \\ u_{n-1} \\ p_o \\ p_1 \\ \vdots \\ \vdots \\ p_{n-1} \end{pmatrix} = \begin{pmatrix} 1 \\ d_1 \\ \vdots \\ \vdots \\ \vdots \\ \vdots \\ \vdots \\ \vdots \\ \vdots \\ d_{2n-1} \end{pmatrix} \tag{11}$$

where the matrix in Eq. (11), known as Sylvester resultant matrix [28], is nonsingular if polynomials $Q(z)$ and $B_{aa'}(z)$ are coprime without common roots. This condition is true if the secondary control path is controllable. When the feedback sensor and actuator are located at the end of the beam, all vibrations modes are controllable and observable. Therefore the secondary path transfer function do not have common roots in $Q(z)$ and $B_{aa'}(z)$. In general, the user can always select the coupling point to avoid vibration nodes and ensure controllability.

Parameter polynomials P(z) and $U(z)$ can be calculated by multiplying the inverse of the Sylvester resultant matrix to both sides of Eq. (11) such that

$$\begin{pmatrix} 1 \\ u_1 \\ \vdots \\ \vdots \\ u_{n-1} \\ p_o \\ p_1 \\ \vdots \\ \vdots \\ p_{n-1} \end{pmatrix} = \begin{pmatrix} 1 & & & & & & & & & & \\ q_1 & 1 & & & & b_0 & & & & & \\ q_2 & q_1 & \ddots & & & b_1 & b_0 & & & & \\ \vdots & q_2 & \ddots & \ddots & & \vdots & b_1 & \ddots & & & \\ \vdots & \vdots & \ddots & \ddots & 1 & \vdots & \vdots & \ddots & \ddots & & \\ q_n & \vdots & \ddots & \ddots & q_1 & b_{n-1} & \vdots & \ddots & \ddots & b_0 & \\ & q_n & \ddots & \ddots & q_2 & & b_{n-1} & \ddots & \ddots & b_1 & \\ & & \ddots & \ddots & \vdots & & & \ddots & \ddots & \vdots & \\ & & & \ddots & \vdots & & & & \ddots & \vdots & \\ & & & & q_n & & & & & b_{n-1} & \end{pmatrix}^{-1} \begin{pmatrix} 1 \\ d_1 \\ \vdots \\ \vdots \\ \vdots \\ \vdots \\ \vdots \\ \vdots \\ \vdots \\ d_{2n-1} \end{pmatrix} \tag{12}$$

It is important to select prototype polynomial $D(z)$ such that whose roots are all inside the unit circle centered at the origin of the complex plane. If the controller is implemented and switched on, it forces the closed-loop transfer function into Eq. (9) such that the closed-loop characteristic equation matches $D(z)$ exactly. Hence the name “pole placement control”. In discrete time control theory [29], closed-loop poles must be inside a unit circle centered at the origin to ensure stability. For a discrete

time system, the closer its poles to the origin of the complex plane, the faster its impulse response converges. Smaller magnitudes of poles imply heavier damping.

In Appendix B, it is shown that $\frac{V_a(z)}{M_{\text{act}}(z)} = \frac{B_{aa'}(z)}{Q(z)}$ is the secondary path transfer function from the moment actuator to the accelerometer feedback sensor. This transfer function can be obtained by offline system identification. Let Rt_i denote the ith root of the polynomials $Q(z)$ and $B_{aa'}(z)$. One may select roots for $D(z)$ on the basis of Rt_i since $Q(z)$ and $B_{aa'}(z)$ are related to the controller parameter polynomials $P(z)$ and $U(z)$ via the Bezout equation in Eq. (10). The first step is to modify or damp Rt_i by

$$\hat{R}t_i = \frac{1}{Rt_i} \times \alpha, \qquad |Rt_i| > 1, \tag{13a}$$

$$\hat{R}t_i = Rt_i \times \alpha, \qquad |Rt_i| < 1. \tag{13b}$$

where α is a parameter used to adjust the damping level introduced to the roots of $Q(z)$ and $B_{aa'}(z)$. The prototype polynomial $D(z)$ is constructed from the modified (damped) roots as

$$D(z) = \frac{1}{z^{2n-1}} \prod_{i=1}^{2n-1} \left(z - \hat{R}t_i\right) = 1 + \sum_{i=1}^{2n-1} d_i z^{-i}. \tag{14}$$

Since a discrete-time system converges more quickly if its closed-loop poles have smaller magnitudes, one may be tempted to select the smallest damping parameter α=0 in order to achieve best damping effects. Both analytical and experimental results indicate that the choice of α is not necessarily the smaller the better for vibration suppression at single or multiple points. It is important to see that $P(z)$ and $U(z)$ contribute to both denominator and numerator of the closed-loop transfer function in Eq. (9), where the numerator is a function of x. If one chooses α=0, the resultant $P(z)$ or $U(z)$ may have some extremely large magnitudes at some frequencies to enhance vibration even if the focus is a single monitor point. The selection of active damping parameter α must balance effects of both numerator and denominator in Eq. (9).

This problem becomes much more complicated if vibrations at multiple points are suppressed. By using one value of α, the controller may have excellent performance at a monitor point, while by selecting other values of α, the controller may have better performance at other monitor points. To achieve the objective of global control, two kinds of sensors are used in the design, implementation and test of the control system. The first kind includes all feedback sensors whose outputs are used by the controller to synthesize the actuation signal. In the proposed HVA, only one feedback sensor is

used to reduce system cost. The second kind sensors are monitor sensors whose outputs are not required for actuation signal synthesis. The monitor signals are used to compare control performance at multiple points. In real practice, it is impossible to use infinite number of monitor sensors to observe the vibration response of entire primary structure. However, it is reasonable to monitor vibration response of the primary structure at finite number of points. One may increase the number of monitor sensors for more accurate approximation of global vibration response, locations of monitor sensors should avoid any node positions and be distributed evenly along the primary structure. During the design process, one may start the damping parameter with α=1 and decrease it with an interval of 0.01 to select the lowest stable value of α. When the damping parameter is set to α=1, it means no damping effect to the modified poles (refer to Eqs. 13a and 13b). Once the lowest stable value of α is found, one may fine tune the damping parameter with an interval of 0.005 to find out the optimal value. The respective mean square velocity, P_x, (detail is discussed in section 6) of each monitor point is calculated and averaged over multiple monitor points. The averaged value is used as a reference to evaluate the global vibration response of the primary structure.

With the help of monitor sensors in the experiments, the optimal value for α was found to be 0.96 for the best and stable vibration attenuation on mean square velocities averaged over multiple monitor points. After comparison of control performance, monitor sensors are uninstalled, leaving the controller operating with its feedback sensor. To the best of Authors' knowledge, the propose HVA is the first one with experimental validation of global vibration control for a beam structure, reported in the literature.

4. SYSTEM IDENTIFICATION

In Appendix B, it is shown that $\frac{V_a(z)}{M_{\text{act}}(z)} = \frac{B_{aa'}(z)}{Q(z)}$ is the transfer function from the moment actuator to the feedback sensor. System identification may be conducted to obtain polynomials $Q(z)$ and $B_{aa'}(z)$ for construction of prototype polynomial $D(z)$ with Eq. (10) and controller design with Eq. (12). Offline system identification is based on input-output data with length N where $N >> 2n$ and n is the order of the identified transfer function. The input signals are white noises generated by the controller to the moment actuator of the HVA. The output signals are measured from the feedback signal simultaneously. Two sequences of discrete time signals with length N can be captured, one sequence $\{m_{act}(1) \quad m_{act}(2) \quad \cdots \quad m_{act}(N)\}$ contains the white noise signals and the other $\{v_a(1) \quad v_a(2) \quad \cdots \quad v_a(N)\}$ contains the vibration feedback signals.

A time-invariant discrete system can be modeled by an *n*th order of difference equation with constant coefficients and an error item [27] as

$$v_a(k)+q_1v_a(k-1)+q_2v_a(k-2)+\cdots+q_nv_a(k-n)$$
$$=b_0m_{act}(k)+b_1m_{act}(k-1)+\cdots+b_{n-1}m_{act}(k-n+1)+e(k) \quad (15)$$

Ideally, if the modeling error is negligible, i.e. $\{e(N)\}=0$, one may take Z-transform on both sides of Eq. (15) to obtain

$$\frac{V_a(z)}{M_{act}(z)}=\frac{b_0+b_1z^{-1}+b_2z^{-2}+\cdots b_{n-1}z^{-n-1}}{1+q_1z^{-1}+q_2z^{-2}+\cdots q_nz^{-n}}=\frac{\sum_{i=0}^{n-1}b_iz^{-i}}{1+\sum_{i=1}^{n}q_iz^{-i}}=\frac{B_{aa'}(z)}{Q(z)} \quad (16)$$

Polynomials $Q(z)$ and $B_{aa'}(z)$ can be obtained when their coefficients b_i and q_i are calculated in the condition of zero error. In practice, modeling error always exists in the identification process to affect the accuracy of the coefficients of $Q(z)$ and $B_{aa'}(z)$. In most applications, it is possible to reduce modeling error $\{e(N)\}$ by matching the measurement data to a system with a higher order *n*. Equation (15) has a matrix-vector representation [27]

$$\begin{bmatrix} v_a(n+1) \\ v_a(n+2) \\ \vdots \\ v_a(N) \end{bmatrix}=\begin{bmatrix} -v_a(n) & \cdots & -v_a(1) & m_{act}(n+1) & \cdots & m_{act}(2) \\ -v_a(n+1) & \cdots & -v_a(2) & m_{act}(n+2) & \cdots & m_{act}(3) \\ \vdots & \vdots & \vdots & \vdots & \vdots & \vdots \\ -v_a(N-1) & \cdots & -v_a(N-n) & m_{act}(N) & \cdots & m_{act}(N-n+1) \end{bmatrix}\begin{bmatrix} q_1 \\ \vdots \\ q_n \\ b_0 \\ \vdots \\ b_{n-1} \end{bmatrix}$$
$$+\begin{bmatrix} e(n+1) \\ e(n+2) \\ \vdots \\ e(N) \end{bmatrix} \quad (17)$$

It can be simplified to

$$y_a=\chi\gamma+e \quad (18)$$

where $y_a=\begin{bmatrix} v_a(n+1) & v_a(n+2) & \cdots & v_a(N) \end{bmatrix}^T$, $\gamma=\begin{bmatrix} q_1 & \cdots & q_n & b_0 & \cdots & b_{n-1} \end{bmatrix}^T$,

$e=\begin{bmatrix} e(n+1) & e(n+2) & \cdots & e(N) \end{bmatrix}^T$ and

$$\chi=\begin{bmatrix} -v_a(n) & \cdots & -v_a(1) & m_{act}(n+1) & \cdots & m_{act}(2) \\ -v_a(n+1) & \cdots & -v_a(2) & m_{act}(n+2) & \cdots & m_{act}(3) \\ \vdots & \vdots & \vdots & \vdots & \vdots & \vdots \\ -v_a(N-1) & \cdots & -v_a(N-n) & m_{act}(N) & \cdots & m_{act}(N-n+1) \end{bmatrix}.$$

Let $\hat{\gamma}$ denote the least-square solution that minimizes modeling error $(y_a - \chi\gamma)^T(y_a - \chi\gamma)$. One may obtain $\hat{\gamma}$ by

$$\hat{\gamma} = (\chi^T\chi)^{-1}\chi^T y_a. \tag{19}$$

To select a proper system order and reduce modeling error, one can plot a figure of least-square modeling error e^Te against the system order *n*. When a proper system order is reached, there should be a dramatic change of the gradient in the plotted curve. In the experiment, the system order was found to be much higher than the number of vibration modes to be suppressed. The large number of system order may be caused by dynamic effect of the equipments, such as anti-aliasing filter, sensor, actuators, amplifiers, A/D and D/A converters. The identified transfer function includes all dynamic effects of experimental equipments in the control loop, in addition to the vibration dynamics of the primary structure.

5. EXPERIMENTAL SETUP

Experiments were conducted to validate the proposed active controller. The equipments setup is shown in Fig. 6, with the following equipments:

1.) dSpace rapid prototype controller board – ds1104 (integrated with A/D and D/A converters)
2.) Alligator anti-alias low-pass filter board – AAF-3PCI (with AAF-3F modules)
3.) Brüel & Kjær Accelerometer – type 4374 (the feedback sensor)
4.) Picomin Accelerometer – model 22 (the monitor sensor)
5.) Brüel & Kjær 4-channel NEXUX charge conditioning amplifier – type 2692 (with double integration function)
6.) Noliac Piezoelectric bender – CMBP06 (two had been used, one for disturbance and one for actuator)
7.) Noliac 1-channel voltage amplifier – NDR 6110 (two had been used for the two piezoelectric benders)

The dSpace ds1104 board was inserted into a host personal computer on which the dSpace ControlDesk software was installed. The sampling frequency of the control system was set to 1720*Hz* and the cut-off frequency of the anti-aliasing filter was tuned to 600*Hz*. In the experiment, the maximum frequency of interest was 520*Hz* which is reasonably less than the anti-aliasing frequency. Typically, sampling size should be two times of the maximum frequency of interest for satisfaction of Nyquist sampling criterion. In real practice, however, oversampling of two times or

more is necessary in order to "cover" the transition band of the anti-aliasing filter. The sample size of each experiment was 40,000. The controller is mathematically given by Eq. (8) and was programmed with the help of dSpace ControlDesk, MatLab Realtime workshop and MatLab Simulink. One could program and implement the controller, design the user-interface and setup experimental parameters via the dSpace ControlDesk. The controller program was compiled via the MatLab Realtime workshop and loaded into the dSpace ds1104 via the dSpace ControlDesk.

A cantilever beam shown in Fig. 7 was used in the experiments as the primary structure. It has dimensions of 150mm (length) × 30mm (width) × 3mm (thickness) with a weight of 0.095kg and was fabricated with mild steel. A piezoelectric bender was adhered to the root side of the primary structure as a disturbance generator (see in Figs. 7 and 9). A stainless steel absorber is shown in Fig. 8 with dimensions of 85mm (length) × 20mm (width) × 1mm (thickness) with a weight of 0.015kg. Its passive resonant frequency was tuned to the first resonant peak of the primary structure. That means the frequency ratio of the absorber to the first primary resonance is equal to 1. A piezoelectric bender was adhered at the root side of the absorber to serve as a moment actuator. The mass ratio between the absorber mass and primary beam structure was 15.8%. The absorber and the accelerometer feedback sensor were mounted at the tip position of the primary cantilever beam as shown in Fig. 9. Another accelerometer sensor was used as a monitor sensor to measure the structural linear velocity response at six different locations as shown in Fig. 9. Measurements of the monitor sensor were collected sequentially at multiple points to evaluate and compare performance of the HVA and its controller.

Signals from both accelerometers were integrated by the 4-channel charge conditioning amplifier to give out linear velocity signals for control and monitor purpose. The dSpace ds1104 controller board was used to generate white noise signal for the disturbance piezoelectric bender, to capture monitor sensor signals for further analysis and to synthesize control signal for the moment actuator of the HVA.

6. EXPERIMENTAL RESULTS AND DISCUSSIONS

Three sets of experiment data were collected to compare the performance of the HVA. The experimental conditions for the three data sets were, respectively, (i) primary structure (beam) only without any control efforts; (ii) control by passive absorber with active controller off and (iii) control by the proposed HVA with active controller on. One monitor sensor was used to measure the linear velocity response at six different positions, respectively and sequentially, at x = 50mm, 70mm, 90mm,

110*mm*, 130*mm* and 150*mm*, as shown in Fig. 9 for each experimental condition and each value of α. The experimental data were used to evaluate and compare the effectiveness of the proposed pole-placement controller on multi-point structural vibration control with respect to its passive counterpart.

For each of three experimental conditions, a set measurement data was obtained that includes 6 sub-sets of monitor data. Each sub-set contains two sequences $\{r(1) \;\; r(2) \;\; \cdots \;\; r(N)\}$ and $\{v_x(1) \;\; v_x(2) \;\; \cdots \;\; v_x(N)\}$ with the same sample size of N=40,000. The first sequence was the white noise disturbance signals and the second sequence was the linear velocity monitor signals measured at position x, for x = 50*mm*, 70*mm*, 90*mm*, 110*mm*, 130*mm* and 150*mm* respectively. These signals were transformed to the frequency domain using MatLAB command "pwelch" and plotted as the normalized power spectral densities (PSD's) $\left|\frac{V(e^{-j\omega\delta t}, x)}{R(e^{-j\omega\delta t})}\right|^2$ (in dB scale) with δt denoted as the sampling time. Due to space limit, PSD's measured at positions x = 50*mm*, 90*mm* and 150*mm* were selected to demonstrate vibration response of the beam structure at far field, middle field and coupling point respectively. Power spectral densities measured at other points were not plotted here as they are similar.

In other words, three PSD's were obtained when the monitor sensor was attached to each of the monitor points to visualize control performance under the three experimental conditions. Take the coupling point x = 150*mm* for example, the PSD's are compared in Fig. 10 for the three experimental conditions. Figure 10a plots the comparison between a raw beam without any vibration control and vibration control with the passive TMD. The TMD is actually a distributed-parameter system with its first resonance pre-tuned to suppress the first resonant peak of the primary structure. With active controller off, the TMD suppressed the first two vibration peaks (78*Hz* and 520*Hz*) of the primary structure but enhanced vibration at other frequencies. Three new peaks were generated by the TMD, two of which sandwich the first peak of the primary structure. These peaks are proportional to the attenuation dip in dB scale. If one increases damping ratio of a TMD to reduce the new peaks, it will deteriorate the attenuation dip sine the TMD requires weak damping to introduce the attenuation dip in the frequency response of the primary structure. Besides, the optimal damping ratio of the TMD depends on accurate knowledge of eigen-functions, resonant frequencies and modal damping ratios of the primary structure. After choosing the optimal damping ratio of a TMD, how to implement it accurately is another practical problem. The proposed HVA is able to attenuate the new peaks without sacrificing the attenuation dip. Figure 10b plots the comparison between vibration control

with the passive TMD and the hybrid HVA. The difference between the two cases was the controller switched off and on. The HVA was able to maintain absorption dips at the first two resonances of the primary structure (78*Hz* and 520*Hz*); and reduced the detrimental effects of the TMD at the two new peaks by more than 8 dB.

The monitor sensor was also attached to other non-coupling points to compare vibration control performance. When the monitor sensor was attached to x = 90*mm*, the corresponding PSD's are shown in Fig. 11. Figure 11a plots the comparison between the raw beam without any vibration control and vibration control with the passive TMD. Again, the TMD suppressed the first two vibration peaks of the primary structure but enhanced vibration at other frequencies. Four new peaks were generated by the TMD, two of which sandwich the first peak of the primary structure. Figure 11b plots the comparison between vibration control with the passive TMD and the hybrid HVA. The HVA was able to maintain absorption at the first two resonances of the primary structure; and reduced the detrimental effects of the TMD at the three new peaks. Particularly, the two lower new peaks, generated by the TMD, were damped down by the HVA by more than 10 dB.

When the monitor sensor was attached to x = 50*mm*, the corresponding PSD's are shown in Fig. 12. Figure 12a plots the comparison between the raw beam without any vibration control and vibration control with the passive TMD. Similar to the PSD's measured at the coupling point, the TMD is seen to suppress the first two vibration peaks of the primary structure but enhanced vibration at other frequencies. Three new peaks were generated by the TMD. Figure 12b plots the comparison between vibration control with the passive TMD and the hybrid HVA. The HVA was able to maintain absorption at the first two resonances of the primary structure; and reduced the detrimental effects of the TMD at all three new peaks.

Let P_x denote the mean square velocity of the beam structure measured at monitor position x. It is calculated as $P_x = (\frac{1}{N})\sum_{i=1}^{N} v_x^2(i)$ for x = 50*mm*, 70*mm*, 90*mm*, 110*mm*, 130*mm* and 150*mm* with the same power of disturbance excitations. When the monitor sensor was attached at each of the above points, the mean square velocities were computed for the cases of (i) raw beam without control (denoted as P_{x_Beam}), (ii) control with passive TMD (active controller switched off) (denoted as P_{x_TMD}), and (iii) control with the proposed HVA (denoted as P_{x_HVA}) with the same power of white noise disturbances. Using Parserval's theorem, one may find that P_{x_Beam}, P_{x_TMD} and P_{x_HVA} are proportional to H_2 norms (areas of PSD's) from the disturbance to monitor point x under different experimental conditions. If plotted in Fig. 13, they can be seen as spatial distributions of H_2 norms

for comparison of vibration control performance under different experimental conditions. Starting from x = 110 *mm*, the detrimental effects of the TMD can be seen with higher values of P_{x_TMD} when the monitor sensor was attached to x = 50*mm*, 70*mm*, 90*mm* and 110*mm*.The proposed HVA, on the other hand, suppressed vibration with lower values of P_{x_HVA} in Fig. 13 when the monitor sensor was attached to all monitor points.

Figure 14 demonstrates the comparison on percentage reduction of the mean square velocity of beam structure at monitor positions x = 50*mm*, 70*mm*, 90*mm*, 110*mm*, 130*mm* and 150*mm* for the cases of (i) passive TMD relative to raw beam (calculated as $\frac{P_{x_Beam} - P_{x_TMD}}{P_{x_Beam}} \times 100\%$), (ii) proposed HVA relative to raw beam (calculated as $\frac{P_{x_Beam} - P_{x_HVA}}{P_{x_Beam}} \times 100\%$), and (iii) proposed HVA relative passive TMD (calculated as $\frac{P_{x_TMD} - P_{x_HVA}}{P_{x_TMD}} \times 100\%$). The passive TMD enhanced the mean square velocity of the primary structure many monitor points, such as x = 50*mm*, 70*mm*, 90*mm*, 110*mm* and it only reduced the velocity at points x = 150*mm* and 130*mm*. This is shown in Fig. 14 where velocity enhancements are indicated by negative values. In contrast, the presented HVA attenuated the mean square velocity of the cantilever beam at all the monitor positions by as much as 93%. Roughly, passive TMD would enhance about 22% of overall mean square velocity of the primary structure in average while the proposed HVA could suppress over 45% in the experiments. It is also critical to see that the presented HVA can provide more than 48% of extra attenuation on the mean square velocity to the primary structure while comparing with passive absorber at all non-coupling locations and as much as 85% at the coupling position. That means the presented HVA has an excellent attenuation capability on the structural vibration response at all the beam span of primary structure for global structural vibration control. The proposed hybrid absorber design can provide a simple alternative for engineers to retrofit the conventional TMD as a higher performance HVA to avoid vibration response enhancement at partial span of the primary structure.

It is shown in Figs. 10-12 that two very high peaks, sandwiching the first resonance peak of the primary structure, were induced by the passive TMD. These new peaks were attenuated significantly by the proposed HVA at all monitor locations. It is clear to see that passive TMD can introduce little damping to the primary structure. The proposed HVA, in contrast, can significantly enhance the damping effect on the two induced resonances of the primary structure.

7. CONCLUSIONS

In many practical applications, eigen-functions and eigen-state feedback of primary structures are not available with sufficient accuracy for the design and stable implementation of active controllers to suppress multi-mode vibrations. It is important to seek alternative methods to design stable active controllers for global and broadband active vibration control in flexible structures. A method is proposed in this study to design and implement a stable active controller for an otherwise passive TMD. The resultant is a HVA that is able to introduce multi-mode damping effects to an entire flexible structure instead of just at the coupling point. The analytical result is validated by experimental tests on a beam structure. In the experiments, the proposed HVA was able to provide more than 48% of extra attenuation on the mean square velocity of the flexible beam when compared with the TMD (difference between turning on/off the active controller) at all non-coupling locations. The improvement was as high as 85% at the coupling point. That means the proposed HVA has an excellent capability to suppress structural vibration of a flexible primary structure for global structural vibration control. The proposed hybrid absorber design can provide a simple and economic alternative for engineers to retrofit the conventional TMD as a higher performance HVA to avoid vibration response enhancement at partial span of the primary structure.

ACKNOWLEDGE

This project was partially supported by internal grant G-U860 from the Hong Kong Polytechnic University.

Appendix A:

Eigen-functions of the primary structure are orthogonal functions. If the primary structure is a beam, its eigen-functions satisfy the following orthogonal equation:

$$\int_{x=0}^{l} \varphi_i(x)\varphi_j(x)\,\mathrm{d}x = \begin{cases} 1 & i = j \quad i,j = 1,2,3\ldots \\ 0 & i \neq j \quad i,j = 1,2,3\ldots \end{cases} \tag{A1}$$

The local modal decomposition is made possible by inner product and written as [30]

$$\eta_i(t) = \int_{x=0}^{l} \varphi_i(x) w(x,t)\mathrm{d}x = \left(\frac{EI}{\rho\omega_i^2}\right)\int_{x=0}^{l} \varphi_i(x) w''''(x,t)\mathrm{d}x, \qquad i = 1,2,3... \tag{A2a}$$

$$\dot{\eta}_i(t) = \left(\frac{CI}{2\xi_i\omega_i\rho}\right)\int_{x=0}^{l} \varphi_i(x) \dot{w}''''(x,t)\mathrm{d}x, \qquad i = 1,2,3... \tag{A2b}$$

where ω_i and ξ_i denotes the damping ratio and the natural frequency of the ith mode of the primary structure. One may substitute Eqs. (4a), (A2a) and (A2b) into Eq. (1) to obtain

$$\ddot{\eta}_i(t) + 2\xi_i\omega_i\dot{\eta}_i(t) + \omega_i^2\eta_i(t) = r(t)\int_0^l \varphi_i(x)\left[\frac{\partial\delta(x-x_d)}{\partial x}\right]dx + \tau(t)\int_0^l \varphi_i(x)\left[\frac{\partial\delta(x-x_a)}{\partial x}\right]\mathrm{d}x$$

$$= -r(t)\,\varphi_i'(x_d) - \tau(t)\,\varphi_i'(x_a) \qquad i = 1,2,3... \tag{A3}$$

Equations (A3), (2) and (3) may be expressed in the Laplace transform domain as another set of dynamic equations for the coupled system:

$$H_i(s) = \frac{-\varphi_{id}' R(s) - \varphi_{ia}' T(s)}{s^2 + 2\xi_i\omega_i s + \omega_i^2}, \qquad i = 1,2,3... \tag{A4}$$

$$T(s) = k[\Phi(s) - \Theta_a(s)] + M_{\text{act}}(s), \tag{A5}$$

$$T(s) = -s^2 J\,\Phi(s) \tag{A6}$$

where $\varphi_{id}' = \varphi_i'(x_d)$ and $\varphi_{ia}' = \varphi_i'(x_a)$; $H_i(s)=\mathcal{L}[\eta_i(t)]$, $R(s)=\mathcal{L}[r(t)]$, $T(s)=\mathcal{L}[\tau(t)]$, $\Phi(s)=\mathcal{L}[\phi(t)]$ and $\Theta_a(s)=\mathcal{L}[\theta_a(t)] =\mathcal{L}[\theta(x_a,t)]$

Substituting Eq. (A4) into the Laplace transformation of Eq. (4c), one may express $\Theta(x_a,s)$, the angular displacement of the beam at the sensor location as:

$$\Theta_a(s) = \Theta(x_a, s)$$

$$= -\sum_{i=1}^{\infty} \varphi_i'(x_a)\,H_i(s) = -\sum_{i=1}^{\infty} \varphi_{ia}'\,H_i(s) = -\sum_{i=1}^{\infty} \varphi_{ia}'\left[\frac{-\varphi_{id}' R(s) - \varphi_{ia}' \mathrm{T}(s)}{s^2 + 2\xi_i\omega_i s + \omega_i^2}\right] \qquad i = 1,2,3\ldots$$

$$= (\varphi'_{\mathrm{a}})^{\mathrm{T}}\,\mathbf{Diag}\left[\frac{1}{s^2+2\xi_i\omega_i s+\omega_i^{\,2}}\right]\left[(\varphi'_{\mathrm{d}})\,R(s)+(\varphi'_{\mathrm{a}})\,\mathrm{T}(s)\right], \qquad i=1,2,3\ldots$$

$$= \frac{B_{a'd'}(s)R(s)+B_{a'a'}(s)\mathrm{T}(s)}{A(s)}, \tag{A7a}$$

where

$$(\varphi'_{\mathrm{a}})^{\mathrm{T}} = [\varphi'_1(x_a) \quad \varphi'_2(x_a) \quad \varphi'_3(x_a) \quad \cdots \quad], \tag{A7b}$$

$$(\varphi'_{\mathrm{d}})^{\mathrm{T}} = [\varphi'_1(x_d) \quad \varphi'_2(x_d) \quad \varphi'_3(x_d) \quad \cdots \quad], \tag{A7c}$$

$$\mathbf{Diag}\left[\frac{1}{s^2+2\xi_i\omega_i s+\omega_i^{\,2}}\right] = \begin{bmatrix} \frac{1}{s^2+2\xi_1\omega_1 s+\omega_1^{\,2}} & 0 & 0 & \cdots & 0 \\ 0 & \frac{1}{s^2+2\xi_2\omega_2 s+\omega_2^{\,2}} & 0 & \cdots & 0 \\ 0 & 0 & \frac{1}{s^2+2\xi_3\omega_3 s+\omega_3^{\,2}} & \cdots & \vdots \\ \vdots & \vdots & \vdots & \ddots & \vdots \\ 0 & 0 & 0 & \cdots & \ddots \end{bmatrix}, \tag{A7d}$$

$$A(s) = \prod_{i=1}^{\infty}\left(s^2+2\xi_i\omega_i s+\omega_i^{\,2}\right), \qquad i = 1,2,3\ldots \tag{A7e}$$

$$B_{a'd'}(s) = A(s)\,(\varphi'_{\mathbf{a}})^{\mathrm{T}}\,\mathbf{Diag}\left[\frac{1}{s^2+2\xi_i\omega_i s+\omega_i^{\,2}}\right](\varphi'_d), \qquad i = 1,2,3\ldots$$

$$= \sum_i\left\{\varphi'_{ia}\;\varphi'_{id}\left[\prod_{k\neq i}\left(s^2+2\xi_k\omega_k s+\omega_k^2\right)\right]\right\}, \qquad i,\,k = 1,2,3\ldots \tag{A7f}$$

$$B_{a'a'}(s) = A(s)\,(\varphi'_{\mathbf{a}})^{\mathrm{T}}\,\mathbf{Diag}\left[\frac{1}{s^2+2\xi_i\omega_i s+\omega_i^{\,2}}\right](\varphi'_{\mathbf{a}}), \qquad i = 1,2,3\ldots$$

$$= \sum_i\left\{\varphi'_{ia}\;\varphi'_{ia}\left[\prod_{k\neq i}\left(s^2+2\xi_k\omega_k s+\omega_k^2\right)\right]\right\}, \qquad i,\,k = 1,2,3\ldots \tag{A7g}$$

Similarly, one may express $V(x_a,s)$, the linear velocity of the beam in terms of the displacement $W(x_a,s)$ at the sensor location as:

$$V_a(s) = V(x_a,s) = sW(x_a,s)$$

$$= s\left[\sum_{i=1}^{\infty}\varphi_i(x_a)H_i(s)\right] = s\left[\sum_{i=1}^{\infty}\varphi_{ia}H_i(s)\right] = s\left\{\sum_{i=1}^{\infty}\varphi_{ia}\left[\frac{-\varphi'_{id}R(s)-\varphi'_{ia}\mathrm{T}(s)}{s^2+2\xi_i\omega_i s+\omega_i^2}\right]\right\}, \quad i=1,2,3\ldots$$

$$= s\left\{(\varphi_{\mathrm{a}})^{\mathrm{T}}\,\mathbf{Diag}\left[\frac{1}{s^2+2\xi_i\omega_i s+\omega_i^{\,2}}\right]\left[-(\varphi'_{\mathrm{d}})\,R(s)-(\varphi'_{\mathrm{a}})\,\mathrm{T}(s)\right]\right\}, \qquad i=1,2,3\ldots$$

$$= \frac{s\left[-B_{ad'}(s)R(s) - B_{aa'}(s)\mathrm{T}(s)\right]}{A(s)}, \tag{A8a}$$

where

$$(\varphi_{\mathrm{a}})^{\mathrm{T}} = [\varphi_1(x_a) \quad \varphi_2(x_a) \quad \varphi_3(x_a) \quad \cdots \quad], \tag{A8b}$$

$$B_{ad'}(s) = A(s)\,(\varphi_{\mathbf{a}})^{\mathrm{T}}\,\mathbf{Diag}\left[\frac{1}{s^2 + 2\xi_i\omega_i s + \omega_i^{\,2}}\right](\varphi'_d), \qquad i = 1,2,3\ldots$$

$$= \sum_i \left\{\varphi_{ia}\ \varphi'_{id}\left[\prod_{k\neq i}\left(s^2 + 2\xi_k\omega_k s + \omega_k^2\right)\right]\right\}, \qquad i,\ k = 1,2,3\ldots \tag{A8c}$$

$$B_{aa'}(s) = A(s)\,(\varphi_{\mathbf{a}})^{\mathrm{T}}\,\mathbf{Diag}\left[\frac{1}{s^2 + 2\xi_i\omega_i s + \omega_i^{\,2}}\right](\varphi'_a), \qquad i = 1,2,3\ldots$$

$$= \sum_i \left\{\varphi_{ia}\ \varphi'_{ia}\left[\prod_{k\neq i}\left(s^2 + 2\xi_k\omega_k s + \omega_k^2\right)\right]\right\}, \qquad i,\ k = 1,2,3\ldots \tag{A8d}$$

One may eliminate $\Phi(s)$ in Eqs. (A5) and (A6), such that

$$T(s) = \frac{s^2}{K(s)}\left[-k\Theta_a(s) + M_{\mathrm{act}}(s)\right] \tag{A9}$$

where $K(s) = s^2 + \frac{k}{J}$ and $M_{\mathrm{act}}(s)$ is the active moment generated by the piezoelectric moment actuator. By substituting Eq. (5) into Eq. (A9), one obtains

$$T(s) = \frac{s^2}{K(s)}\left[-k\Theta_a(s) + G(s)V_a(s)\right] \tag{A10}$$

A further substitution of Eqs. (A7a) and (A8a) into Eq. (A10) leads to

$$T(s) = \frac{s^2}{K(s)}\left\{\frac{-k}{A(s)}\left[B_{a'd'}(s)R(s) + B_{a'a'}(s)\mathrm{T}(s)\right] + \frac{sG(s)}{A(s)}\left[-B_{ad'}(s)R(s) - B_{aa'}(s)\mathrm{T}(s)\right]\right\}$$

$$= \frac{-\left[s^2kB_{a'd'}(s) + s^3G(s)B_{ad'}(s)\right]R(s) - \left[s^2kB_{a'a'}(s) + s^3G(s)B_{aa'}(s)\right]\mathrm{T}(s)}{A(s)K(s)}$$

$$= -\frac{\left[s^2kB_{a'd'}(s) + s^3G(s)B_{ad'}(s)\right]R(s)}{A(s)K(s) + s^2kB_{a'a'}(s) + s^3G(s)B_{aa'}(s)} \tag{A11}$$

Recall Eq. (A4) and substitute it into Laplace transformation of Eq. (4b), one may obtain

$$V(x,s) = sW(x,s) = s\left[\sum_{i=1}^{\infty}\varphi_{ix}H_i(s)\right] = s\left\{\sum_{i=1}^{\infty}\varphi_{ix}\left[\frac{-\varphi'_{id}R(s)-\varphi'_{ia}T(s)}{s^2+2\xi_i\omega_i s+\omega_i^2}\right]\right\}, \qquad i=1,2,3\ldots$$

$$= s\left\{(\varphi_{\mathrm{x}})^{\mathrm{T}}\,\mathbf{Diag}\left[\frac{1}{s^2+2\xi_i\omega_i s+{\omega_i}^2}\right]\left[-(\varphi'_{\mathrm{d}})\,R(s)-(\varphi'_{\mathrm{a}})\,T(s)\right]\right\}, \qquad i=1,2,3\ldots$$

$$= \frac{s\left[-B_{xd'}(s)R(s)-B_{xa'}(s)T(s)\right]}{A(s)}$$

$$= -\frac{sB_{xd'}(s)R(s)}{A(s)} - \frac{sB_{xa'}(s)}{A(s)}\left\{-\frac{\left[s^2kB_{a'd'}(s)+s^3G(s)B_{ad'}(s)\right]R(s)}{A(s)K(s)+s^2kB_{a'a'}(s)+s^3G(s)B_{aa'}(s)}\right\} \qquad \text{(A12)}$$

The above equation is equivalent to

$$\frac{V(x,s)}{R(s)} = \frac{-sA(s)K(s)B_{xd'}(s)+s^3k[-B_{xd'}(s)B_{a'a'}(s)+B_{xa'}(s)B_{a'd'}(s)]}{A(s)[A(s)K(s)+s^2kB_{a'a'}(s)+s^3G(s)B_{aa'}(s)]}$$

$$+\frac{s^4G(s)[-B_{xd'}(s)B_{aa'}(s)+B_{xa'}(s)B_{ad'}(s)]}{A(s)[A(s)K(s)+s^2kB_{a'a'}(s)+s^3G(s)B_{aa'}(s)]}$$

$$= \frac{-sA(s)K(s)B_{xd'}(s)+s^3kA(s)\Delta B_k(s)+s^4G(s)A(s)\Delta B_G(s)}{A(s)[A(s)K(s)+s^2kB_{a'a'}(s)+s^3G(s)B_{aa'}(s)]}$$

$$= \frac{-sK(s)B_{xd'}(s)+s^3k\Delta B_k(s)+s^4G(s)\Delta B_G(s)}{A(s)K(s)+s^2kB_{a'a'}(s)+s^3G(s)B_{aa'}(s)} \qquad \text{(A13)}$$

where

$$B_{xd'}(s) = A(s)\,(\varphi_x)^{\mathrm{T}}\,\mathbf{Diag}\left[\frac{1}{s^2+2\xi_i\omega_i s+{\omega_i}^2}\right](\varphi'_d), \qquad i=1,2,3\ldots$$

$$= \sum_i\left\{\varphi_{ix}\,\varphi_{id'}\left[\prod_{k=1,k\neq i}^{\infty}\left(s^2+2\xi_k\omega_k s+\omega_k^2\right)\right]\right\}, \qquad i,k=1,2,3\ldots \qquad \text{(A14a)}$$

$$B_{xa'}(s) = A(s)\,(\varphi_x)^{\mathrm{T}}\,\mathbf{Diag}\left[\frac{1}{s^2+2\xi_i\omega_i s+{\omega_i}^2}\right](\varphi'_a), \qquad i=1,2,3\ldots$$

$$= \sum_i\left\{\varphi_{ix}\,\varphi_{ia'}\left[\prod_{k=1,k\neq i}^{\infty}\left(s^2+2\xi_k\omega_k s+\omega_k^2\right)\right]\right\}, \qquad i,k=1,2,3\ldots \qquad \text{(A14b)}$$

$$\Delta B_k(s) = \sum_i\left\{\varphi_{ix}\,\varphi_{ia'}\sum_{j=1,j\neq i}^{\infty}\left[\varphi_{ja'}\varphi_{jd'}\prod_{k=1,k\neq j\neq i}^{\infty}\left(s^2+2\xi_k\omega_k s+\omega_k^2\right)\right]\right\},$$

$$-\sum_i\left\{\varphi_{ix}\,\varphi_{id'}\sum_{j=1,j\neq i}^{\infty}\left[\varphi_{ja'}\varphi_{ja'}\prod_{k=1,k\neq j\neq i}^{\infty}\left(s^2+2\xi_k\omega_k s+\omega_k^2\right)\right]\right\} \qquad i,j,k=1,2,3\ldots \qquad \text{(A14c)}$$

$$\Delta B_G(s) = \sum_i \left\{ \varphi_{ix}\, \varphi_{ia'} \sum_{j=1,\, j\neq i}^{\infty} \left[\varphi_{ja} \varphi_{jd'} \prod_{k=1, k\neq j\neq i}^{\infty} \left(s^2 + 2\xi_k \omega_k s + \omega_k^2 \right) \right] \right\},$$

$$- \sum_i \left\{ \varphi_{ix}\, \varphi_{id'} \sum_{j=1,\, j\neq i}^{\infty} \left[\varphi_{ja} \varphi_{ja'} \prod_{k=1, k\neq j\neq i}^{\infty} \left(s^2 + 2\xi_k \omega_k s + \omega_k^2 \right) \right] \right\} \qquad i, j, k = 1,2,3\ldots \qquad \text{(A14d)}$$

This is the closed-loop transfer function from the disturbance to any location x of the primary system (the beam).

Appendix B

Recall Eq. (A9) and substitute it into Eq. (A8a), one may obtain

$$V_a(s) = V(x_a, s) = sW(x_a, s) = \frac{-sB_{ad'}(s)R(s)}{A(s)} - \frac{sB_{aa'}(s)}{A(s)}\left[\frac{s^2}{K(s)}\left(-k\Theta_a(s) + M_{\text{act}}(s)\right)\right]$$

$$= \frac{-sB_{ad'}(s)R(s)}{A(s)} + \left[\frac{s^3 kB_{aa'}(s)}{A(s)K(s)}\right]\Theta_a(s) - \left[\frac{s^3 B_{aa'}(s)}{A(s)K(s)}\right]M_{\text{act}}(s) \tag{B1}$$

One may eliminate the disturbance signal, i.e. $R(s)$=0, during system identification and rewrite Eq. (B1) as

$$V_a(s) = \left[\frac{s^3 kB_{aa'}(s)}{A(s)K(s)}\right]\Theta_a(s) - \left[\frac{s^3 B_{aa'}(s)}{A(s)K(s)}\right]M_{\text{act}}(s) \tag{B2}$$

Similarly, one may substitute Eq. (A9) into Eq. (A7a) and eliminate disturbance signal, i.e. $R(s)$=0 to obtain

$$\Theta_a(s) = \Theta(x_a, s) = \frac{B_{a'a'}(s)}{A(s)}\left[\frac{s^2}{K(s)}\left(-k\Theta_a(s) + M_{\text{act}}(s)\right)\right]$$

$$= \left[\frac{s^2 B_{a'a'}(s)}{A(s)K(s) + s^2 kB_{a'a'}(s)}\right]M_{\text{act}}(s) \tag{B3}$$

Now substituting Eq. (B3) into Eq. (B2), one may obtain

$$V_a(s) = \left[\frac{s^3 kB_{aa'}(s)}{A(s)K(s)}\right]\left[\frac{s^2 B_{a'a'}(s)}{A(s)K(s) + s^2 kB_{a'a'}(s)}\right]M_{\text{act}}(s) - \left[\frac{s^3 B_{aa'}(s)}{A(s)K(s)}\right]M_{\text{act}}(s)$$

$$= \left\{\frac{[s^3 kB_{aa'}(s)][s^2 B_{a'a'}(s)] - [s^3 B_{aa'}(s)][A(s)K(s) + s^2 kB_{a'a'}(s)]}{[A(s)K(s)][A(s)K(s) + s^2 kB_{a'a'}(s)]}\right\}M_{\text{act}}(s)$$

$$= \left[\frac{-s^3 B_{aa'}(s)}{A(s)K(s) + s^2 kB_{a'a'}(s)}\right]M_{\text{act}}(s) \tag{B4}$$

According to Eq. (B4) the transfer function from the moment actuator to the feedback sensor can be rewritten as

$$\frac{V_a(z)}{M_{\text{act}}(z)} = \frac{B_{aa'}(z)}{A(z)K(z) + kB_{a'a'}(z)} = \frac{B_{aa'}(z)}{Q(z)}. \tag{B5}$$

REFERENCES

1. A. Occhiuzzi, Additional viscous dampers for civil structures: Analysis of design methods based on effective evaluation of modal damping ratios. *Engineering Structures* 31 (2009) 1093-1101.
2. E. Aydin, M.H. Boduroglu, and D. Guney, Optimal damper distribution for seismic rehabilitation of planar building structures. *Engineering Structures* 29 (2007) 176-185.
3. C.C. Chang, Mass dampers and their optimal designs for building vibration control. *Engineering Structures* 21 (1999) 454-463.
4. F. Weber, G. Feltrin, M. Maslanka, W. Fobo, and H. Distl, Design of viscous dampers targeting multiple cable modes. *Engineering Structures* 31 (2009) 2797-2800.
5. X.Y. Wang, Y.Q. Ni, J.M. Ko, and Z.Q. Chen, Optimal design of viscous dampers for multi-mode vibration control of bridge cables. *Engineering Structures* 27 (2005) 792-800.
6. A.A. Taflanidis, D.C. Angelides, and G.C. Manos, Optimal design and performance of liquid column mass dampers for rotational vibration control of structures under white noise excitation, *Engineering Structures* 27 (4):(2005) 524-534.
7. R.G. Jacquot, The spatial average mean square motion as an objective function for optimizing damping in damped modified systems. *Journal of Sound and Vibration* 259 (2003) 955-965.
8. D. Karnopp, Active and semi-active vibration isolation. *Journal of Mechanical Design, Trans. ASME* 117 (1995) 177-185.
9. J.P. Den Hartog, Mechanical vibrations. *McGraw Hill, New York* (1956).
10. D.J. Inman, Engineering vibrations. *Prentice-Hill, NJ* (1994).
11. F. Hermann, Device for damping vibrations of bridges. *German Patent 525455* (1909).
12. T. Taniguchi, A. Der Kiureghian, and M. Melkumyan, Effect of tuned mass damper on displacement demand of base-isolated structures. *Engineering Structures* 30 (2008) 3478-3488.
13. Z. Zhang and T. Balendra, Passive control of bilinear hysteretic structures by tuned mass damper for narrow band seismic motions. *Engineering Structures* 54 (2013) 103-111.
14. I.M. Díaz, E. Pereira, M.J. Hudson, and P. Reynolds, Enhancing active vibration control of pedestrian structures using inertial actuators with local feedback control. *Engineering Structures* 41 (2012) 157-166.
15. W.O. Wong and Y.L. Cheung, Optimal design of a damped dynamic vibration absorber for vibration control of structure excited by ground motion. *Engineering Structures* 30 (2008) 282-286.

16. J.Q. Sun, M.R. Jolly, and M.A. Norris, Passive, adaptive and active tuned vibration absorbers---a survey. *Journal of Mechanical Design* 117 (1995) 234-242.
17. R.A. Burdisso and J.D. Heilmann, A new dual-reaction mass dynamic vibration absorber actuator for active vibration control. *Journal of Sound and Vibration* 214 (1998) 817-831.
18. S.T. Wu, Y.Y. Chiu, and Y.C. Yeh, Hybrid vibration absorber with virtual passive devices. *Journal of Sound and Vibration* 299 (2007) 247-260.
19. K.C.S. Kwok and B. Samali, Performance of tuned mass dampers under wind loads. *Engineering Structures* 17 (1995) 655-667.
20. N. Olgac and B.T. Holm Hansen, A novel active vibration absorption technique: delayed resonator. *Journal of Sound and Vibration* 176 (1994) 93-104.
21. J.C.H. Chang and T.T. Soong, Structural control using active tuned mass dampers. *Journal of the Engineering Mechanics Division, ASCE* 106 (1980) 1091-1098.
22. S.J. Huang and W.C. Lin, Adaptive fuzzy controller with sliding surface for vehicle suspension control. *Fuzzy Systems, IEEE Transactions on* 11 (2003) 550-559.
23. M.H. Tso, J. Yuan, and W.O. Wong, Suppression of random vibration in flexible structures using a hybrid vibration absorber. *Journal of Sound and Vibration* 331 (2012) 974-986.
24. K. Ito and S. Nakagiri, Identifiability of stiffness and damping coefficients in Euler-Bernoulli beam equations with Kelvin-Voigt damping. *Numerical Functional Analysis and Optimization* 18 (1997) 107-129.
25. W.O. Wong, S.L. Tang, Y.L. Cheung, and L. Cheng, Design of a dynamic vibration absorber for vibration isolation of beams under point or distributed loading. *Journal of Sound and Vibration* 301 (2007) 898-908.
26. J.S. Hwang, J. Kim, and Y.M. Kim, Rotational inertia dampers with toggle bracing for vibration control of a building structure. *Engineering Structures* 29 (2007) 1201-1208.
27. T.C. Hsia, *System Identification: Least-Squares Methods*. 1977: Lexington Books , D. C. Heath and Company, Lexington, Massachusetts Toronto.
28. G.C. Goodwin, *Adaptive filtering prediction and control*, ed. K.S. Sin. 1984, Englewood Cliffs, N.J: Prentice-Hall.
29. K. Ogata, *Modern Control Engineering*. 2001: Prentice Hall, PTR, Upper Saddle River, NJ.
30. H.T. Banks, Z.-H. Luo, L.A. Bergman, and D.J. Inman, On the Existence of Normal Modes of Damped Discrete-Continuous Systems. *Journal of Applied Mechanics* 65 (1998) 980-989.

Figure Captions:

Fig. 1 2D schematic of a tuned mass damper used in many skyscrapers like the “Taipei 101”.

Fig. 2 Cantilever beam coupled with the proposed hybrid vibration absorber (HVA) at point $x = x_a$ under an external moment excitation $r(t)\delta(x - x_d)$ at point $x = x_d$.

Fig. 3 Schematic of the equivalent moment.

Fig. 4 Schematic of a conventional hybrid vibration absorber.

Fig. 5 Schematic of the proposed hybrid vibration absorber.

Fig. 6 Schematic of the experimental setup.

Fig. 7 Figure of the proposed hybrid vibration absorber coupled at the tip position of a primary cantilever beam with a piezoelectric bender adhered at the cantilever root side as moment disturbance.

Fig. 8 Figure of the proposed hybrid vibration absorber with a piezoelectric bender adhered at its root side as moment actuator for control purpose and a tunable screw-washer-nut set as absorber mass.

Fig. 9 Schematic of the monitor positions for structural vibration response measurement.

Fig. 10. Comparison of PSD, $\left|\frac{V(e^{-j\omega\delta t}, x)}{R(e^{-j\omega\delta t})}\right|^2$, measured at x=150mm of the primary structure:

(a) ——— raw beam; ——— with passive TMD; and

(b) ——— with passive TMD; ——— with proposed HVA.

Fig. 11. Comparison of PSD, $\left|\frac{V(e^{-j\omega\delta t},x)}{R(e^{-j\omega\delta t})}\right|^2$, measured at x=90mm of the primary structure:

(a) ——— raw beam; ——— with passive TMD; and

(b) ——— with passive TMD; ——— with proposed HVA.

Fig. 12. Comparison of PSD, $\left|\frac{V(e^{-j\omega\delta t},x)}{R(e^{-j\omega\delta t})}\right|^2$, measured at x=50mm of the primary structure:

(a) ——— raw beam; ——— with passive TMD; and

(b) ——— with passive TMD; ——— with proposed HVA.

Fig. 13. Mean square velocity, $P_x = (\frac{1}{N})\sum_{i=1}^{N} v_x^2(i)$, of the beam structure in Fig. 9 measured at x=150mm, 130mm, 110mm, 90mm, 70mm, 50mm and the spatial average value for the cases of

(i) ■ raw beam (P_{x_Beam}),

(ii) ■ control with passive TMD (P_{x_TMD}), and

(iii) □ control with the proposed HVA (P_{x_HVA}).

Fig. 14 Comparison of the percentage reduction of mean square velocity of the beam structure measured at x = 150mm, 130mm, 110mm, 90mm, 70mm, 50mm and the spatial average value for the cases of

(i) ■ passive TMD relative to raw beam, $\frac{(P_{x_Beam} - P_{x_TMD})}{P_{x_Beam}} \times 100\%$,

(ii) □ proposed HVA relative to raw beam, $\frac{(P_{x_Beam} - P_{x_HVA})}{P_{x_Beam}} \times 100\%$, and

(iii) ■ proposed HVA relative to passive TMD, $\frac{(P_{x_TMD} - P_{x_HVA})}{P_{x_TMD}} \times 100\%$.

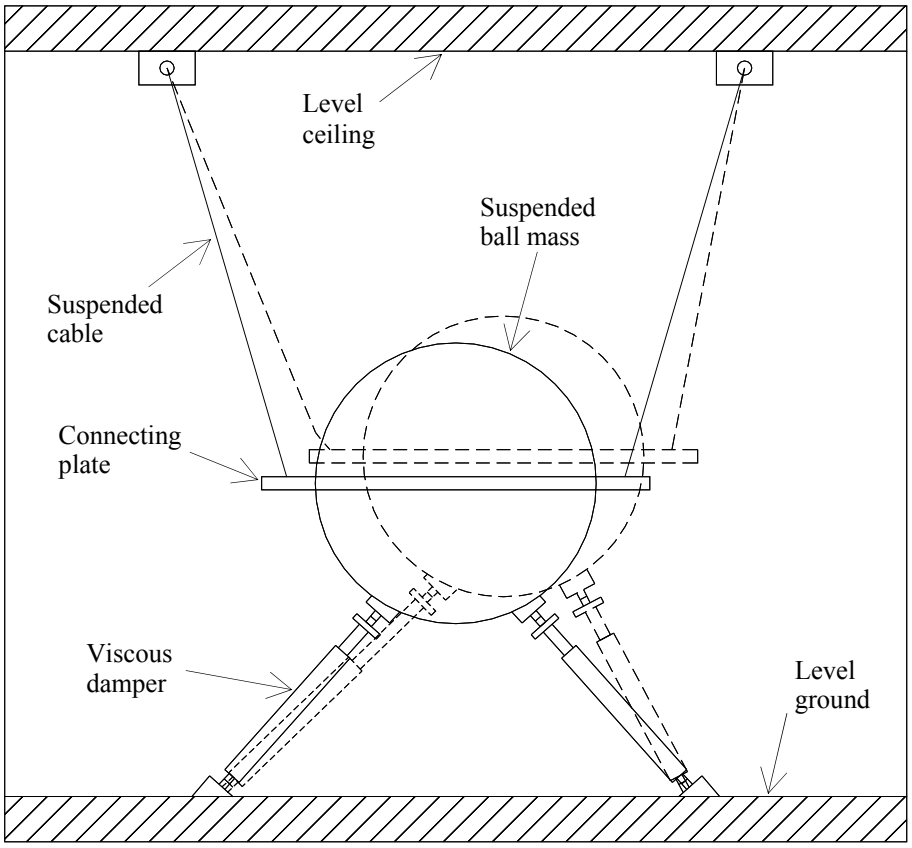

Fig. 1. 2D schematic of a tuned mass damper used in many skyscrapers like the “Taipei 101”.

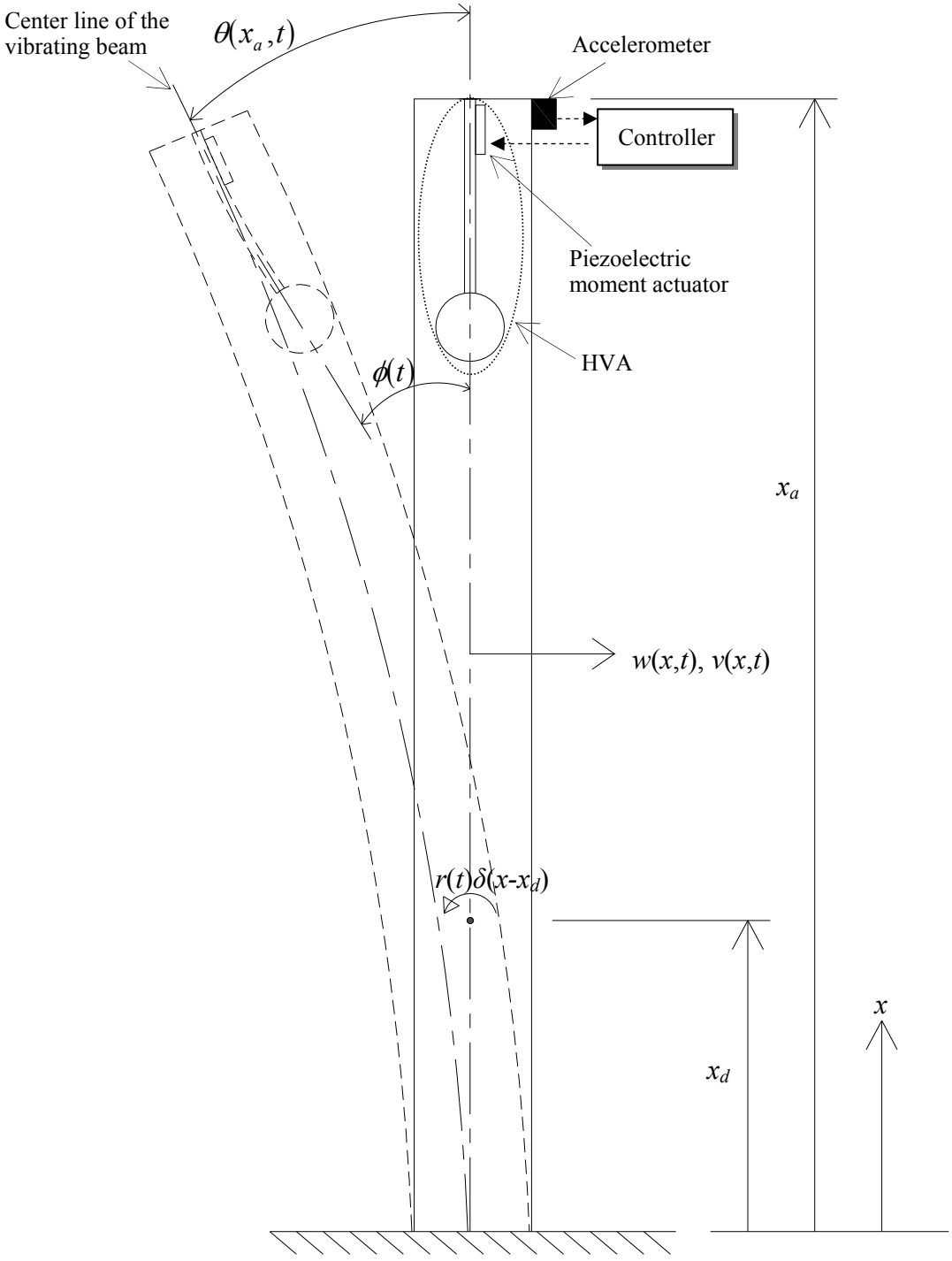

Fig. 2. Cantilever beam coupled with the proposed hybrid vibration absorber (HVA) at point $x = x_a$ under an external moment excitation $r(t)\delta(x - x_d)$ at point $x = x_d$.

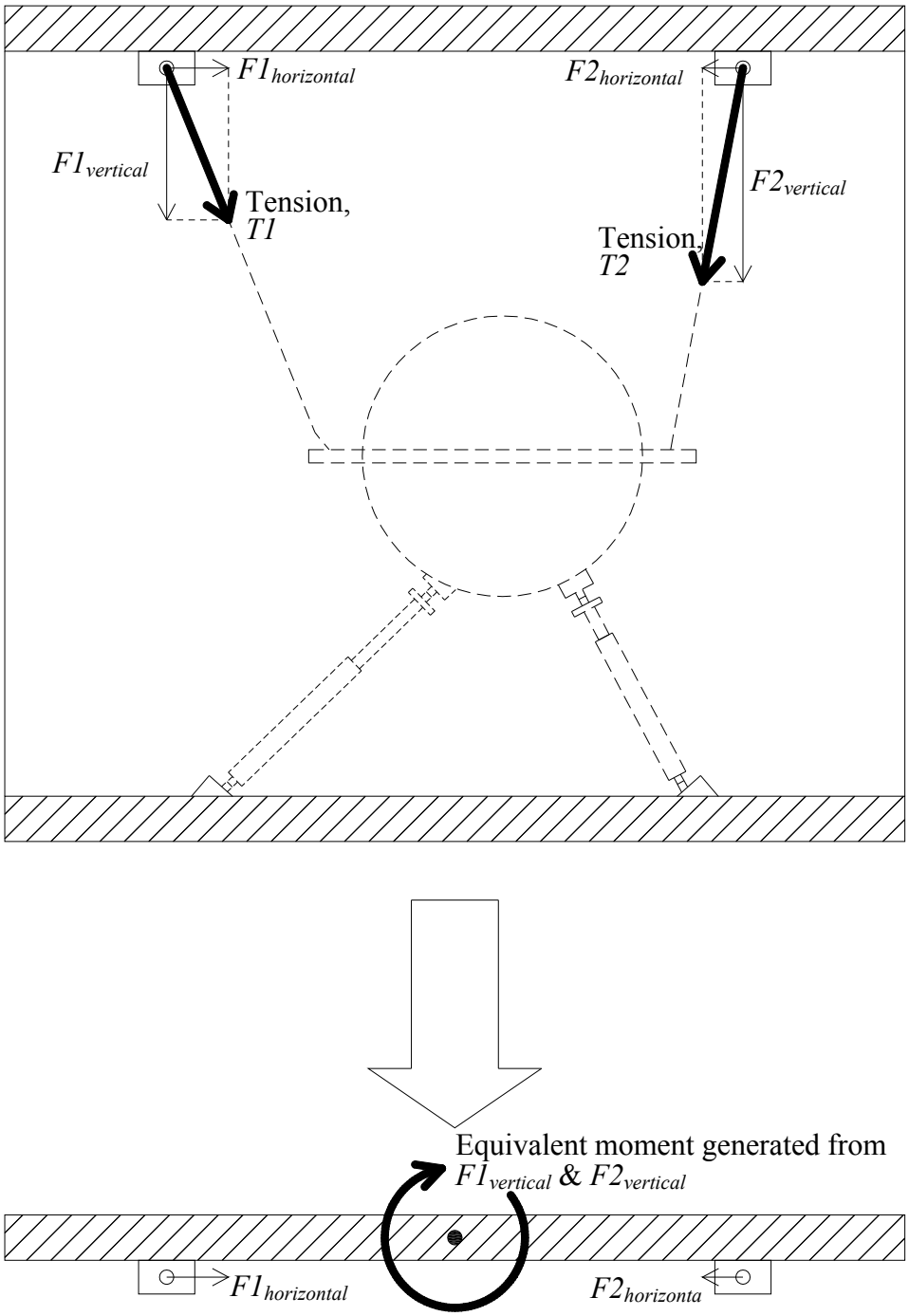

Fig. 3. Schematic of the equivalent moment.

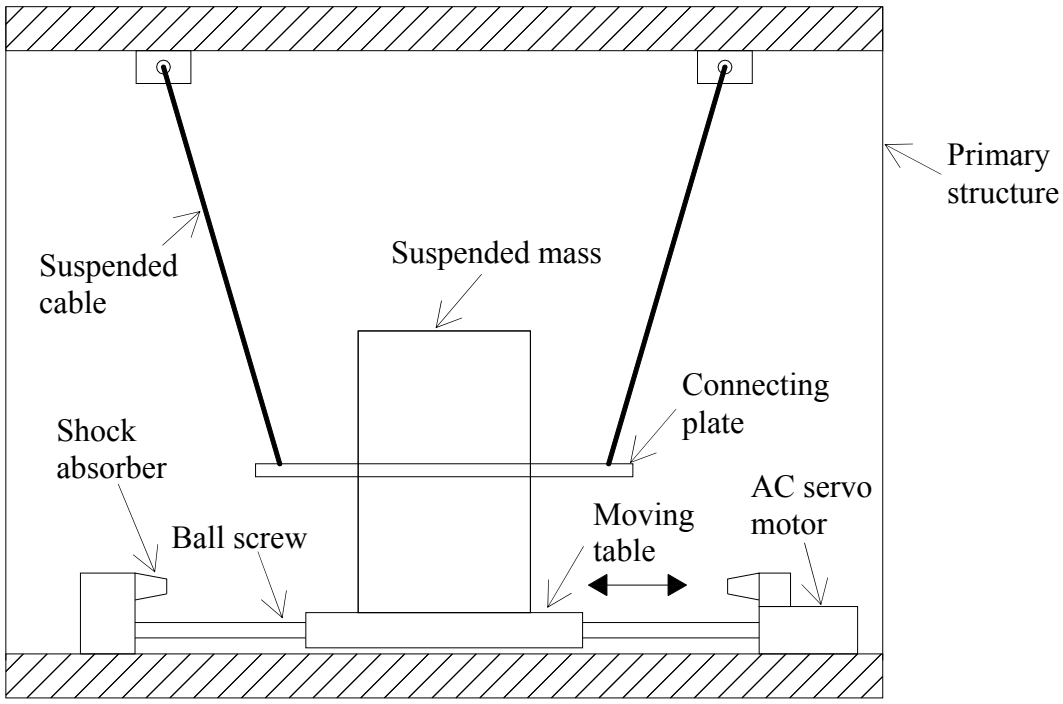

Fig. 4. Schematic of a conventional hybrid vibration absorber.

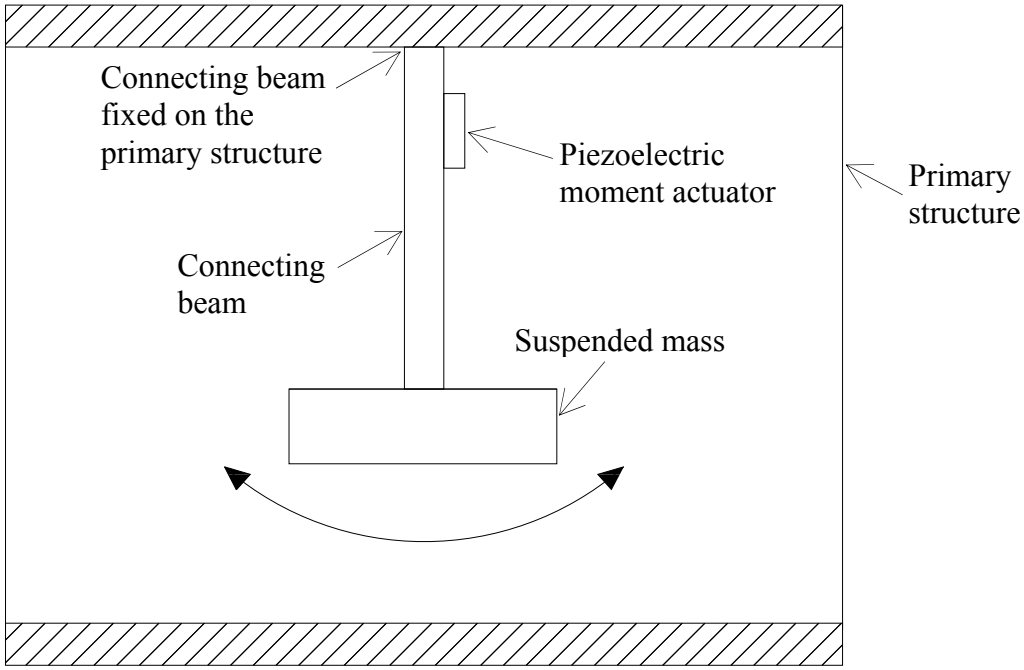

Fig. 5. Schematic of the proposed hybrid vibration absorber.

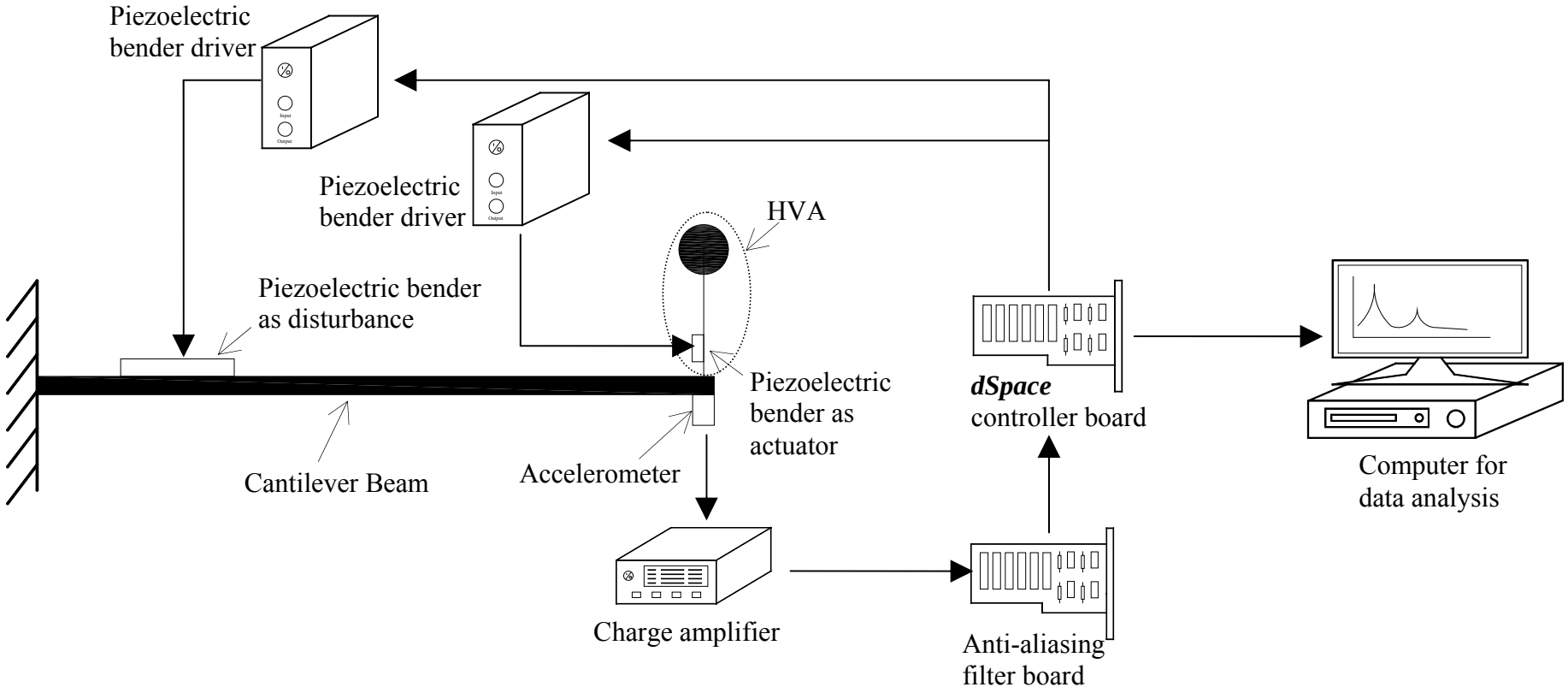

Fig. 6. Schematic of the experimental setup.

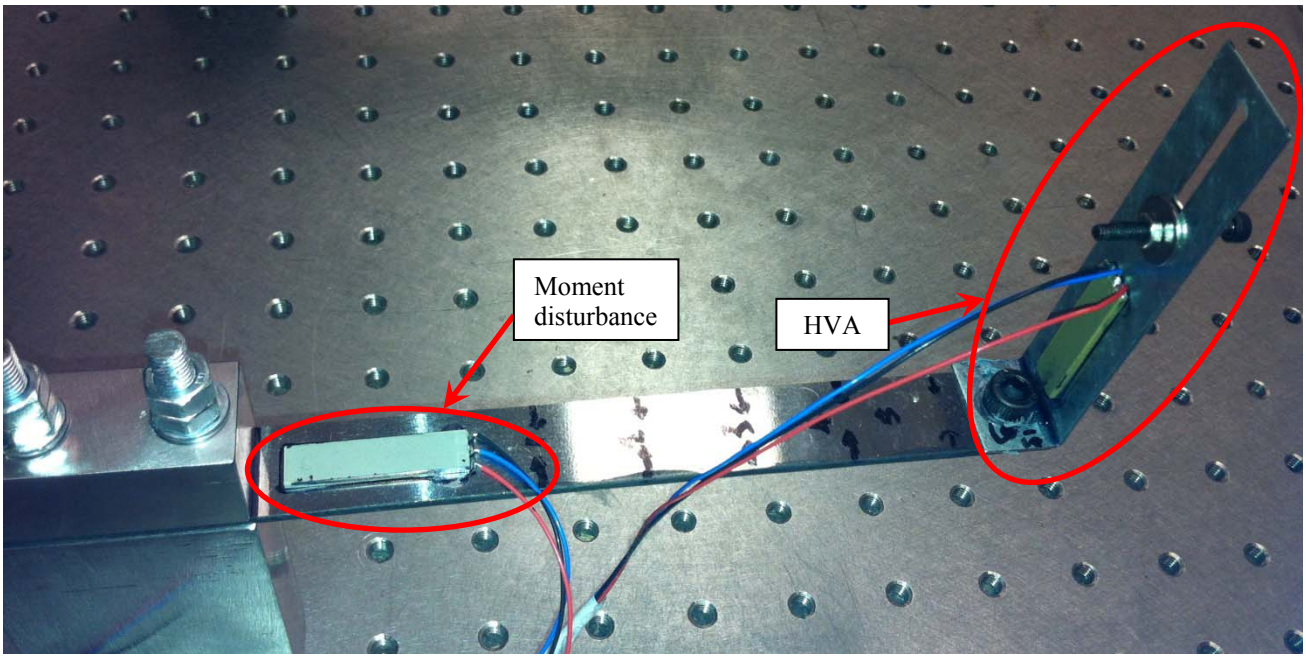

Fig. 7. Figure of the proposed hybrid vibration absorber coupled at the tip position of a primary cantilever beam with a piezoelectric bender adhered at the cantilever root side as moment disturbance.

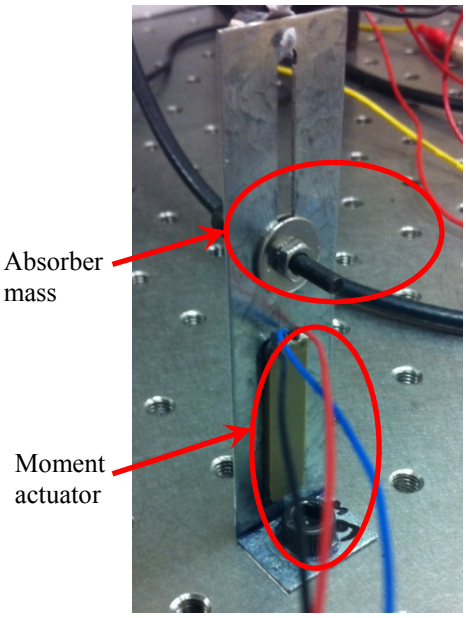

Fig. 8. Figure of the proposed hybrid vibration absorber with a piezoelectric bender adhered at its root side as moment actuator for control purpose and a tunable screw-washer-nut set as absorber mass.

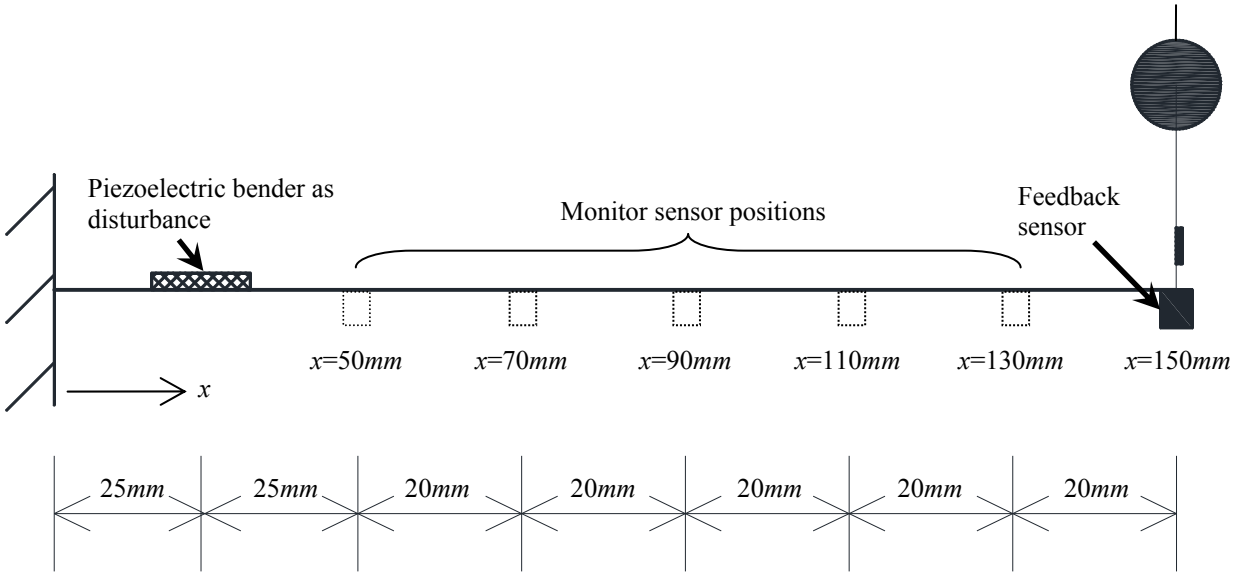

Fig. 9. Schematic of the monitor positions for structural vibration response measurement.

a)

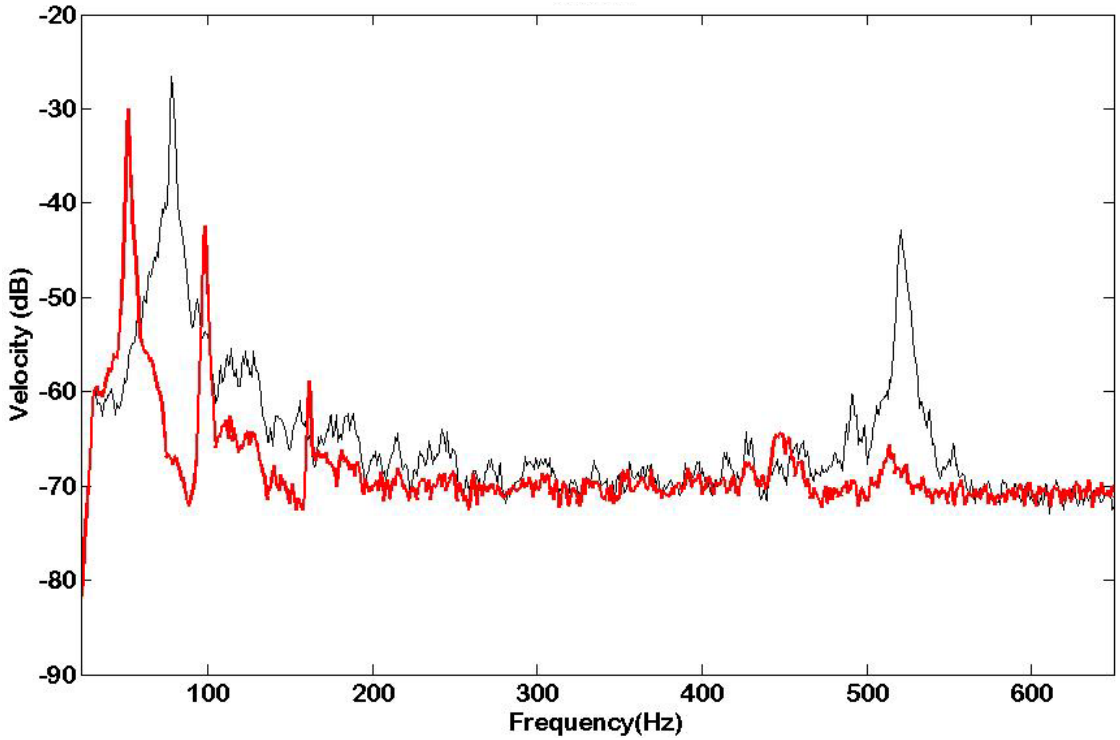

b)

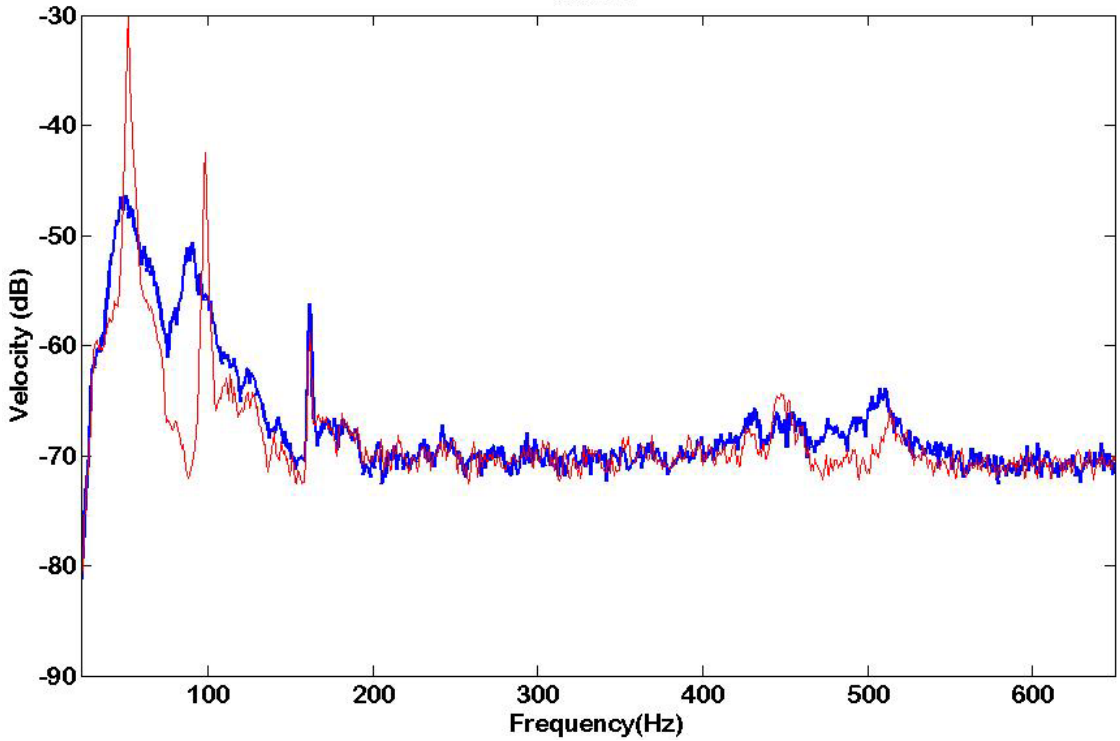

Fig. 10. Comparison of PSD, $\left|\frac{V(e^{-j\omega\delta t},x)}{R(e^{-j\omega\delta t})}\right|^2$, measured at x=150mm of the primary structure:

(a) ——— raw beam; ——— with passive TMD; and

(b) ——— with passive TMD; ——— with proposed HVA.

a)

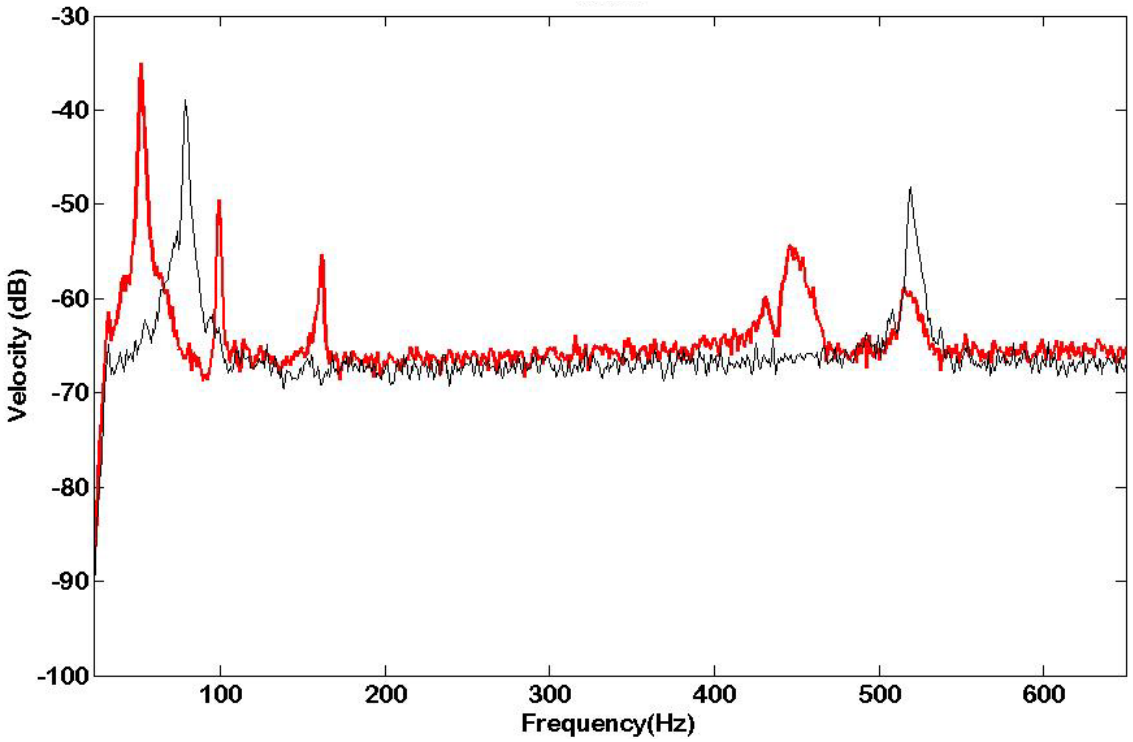

b)

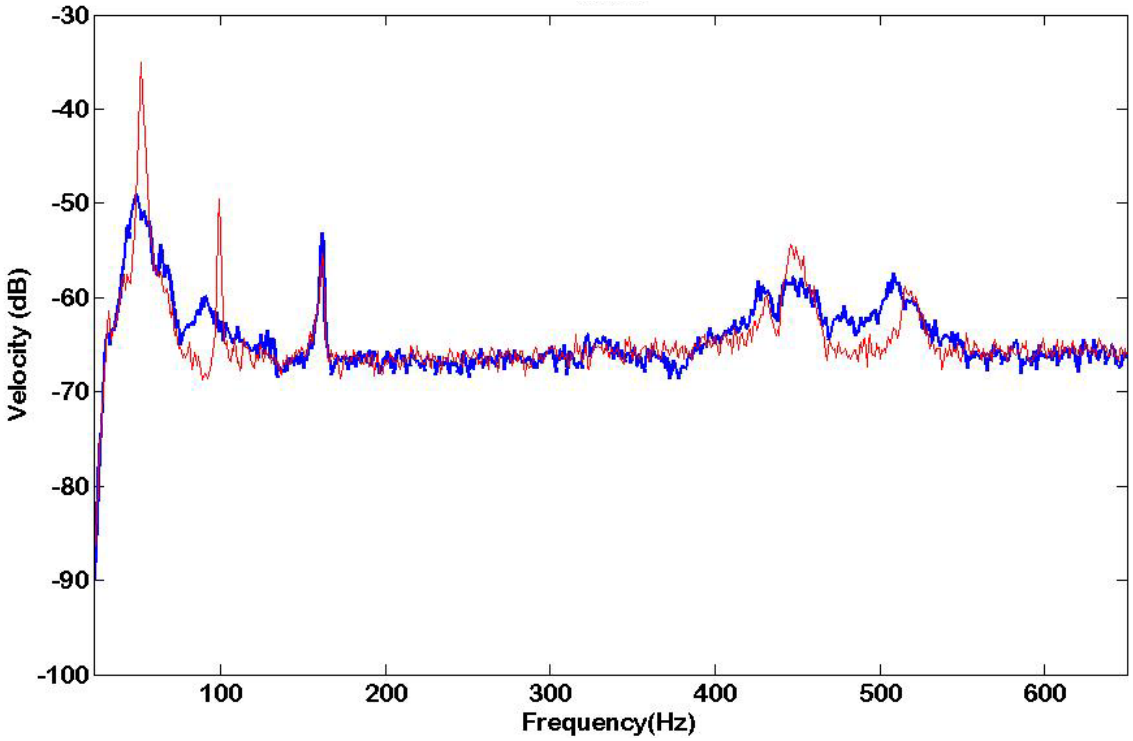

Fig. 11. Comparison of PSD, $\left|\frac{V(e^{-j\omega\delta t},x)}{R(e^{-j\omega\delta t})}\right|^2$,measured at x=90mm of the primary structure:

(a) ——— raw beam; ━━━ with passive TMD; and

(b) ——— with passive TMD; ━━━ with proposed HVA.

a)

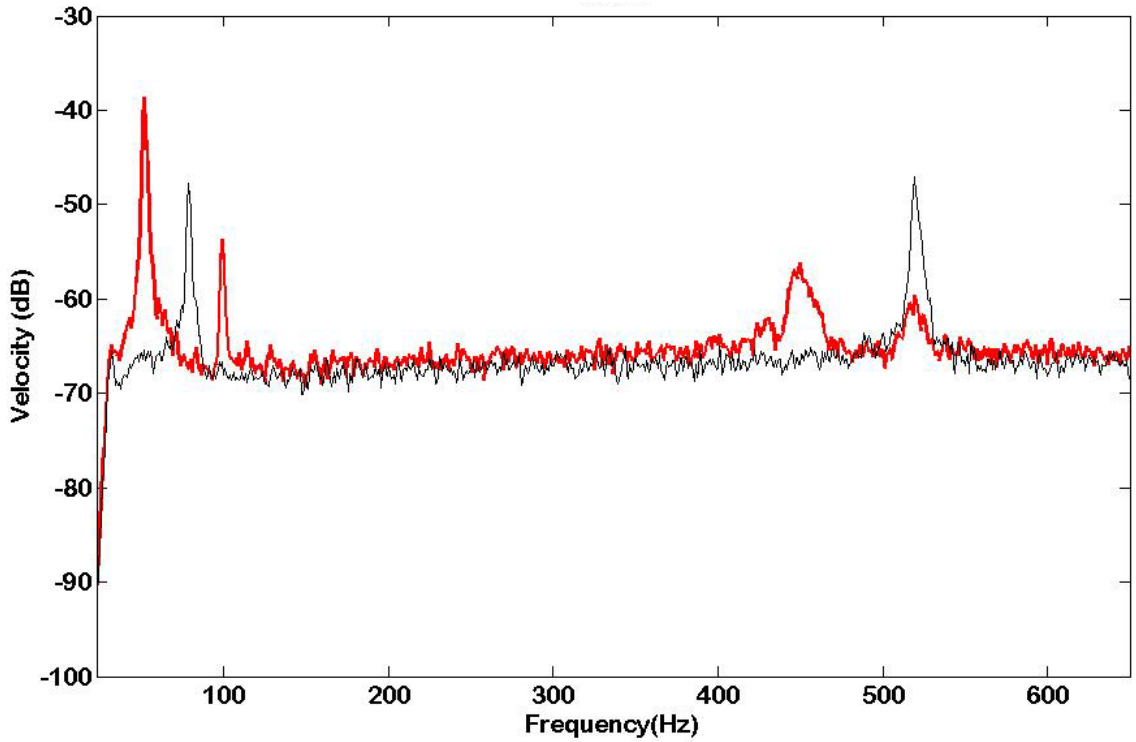

b)

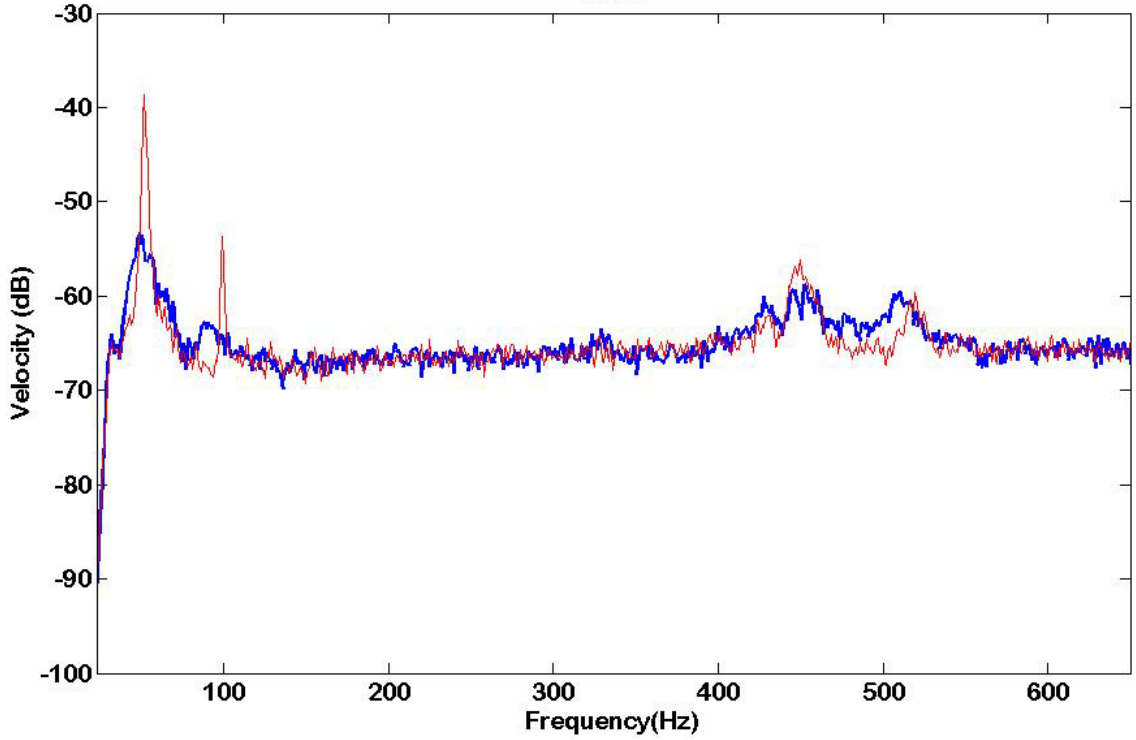

Fig. 12. Comparison of PSD, $\left|\frac{V(e^{-j\omega\delta t},x)}{R(e^{-j\omega\delta t})}\right|^2$, measured at x=50mm of the primary structure:

(a) ——— raw beam; ——— with passive TMD; and

(b) ——— with passive TMD; ——— with proposed HVA.

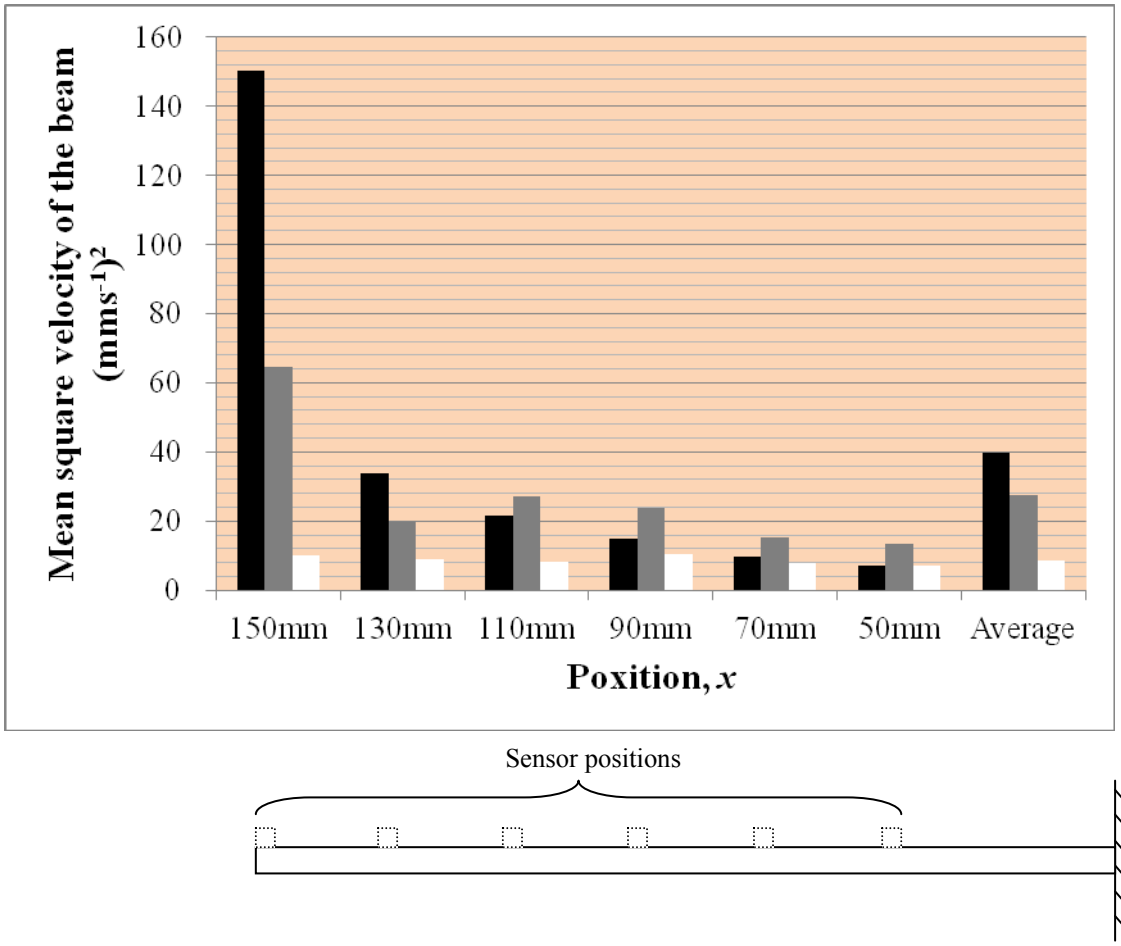

Fig. 13. Mean square velocity, $P_x = (\frac{1}{N})\sum_{i=1}^{N} v_x^2(i)$, of the beam structure in Fig. 9 measured at x = 150mm, 130mm, 110mm, 90mm, 70mm, 50mm and the spatial average value for the cases of

(i) raw beam (P_{x_Beam}),

(ii) control with passive TMD (P_{x_TMD}), and

(iii) control with the proposed HVA (P_{x_HVA}).

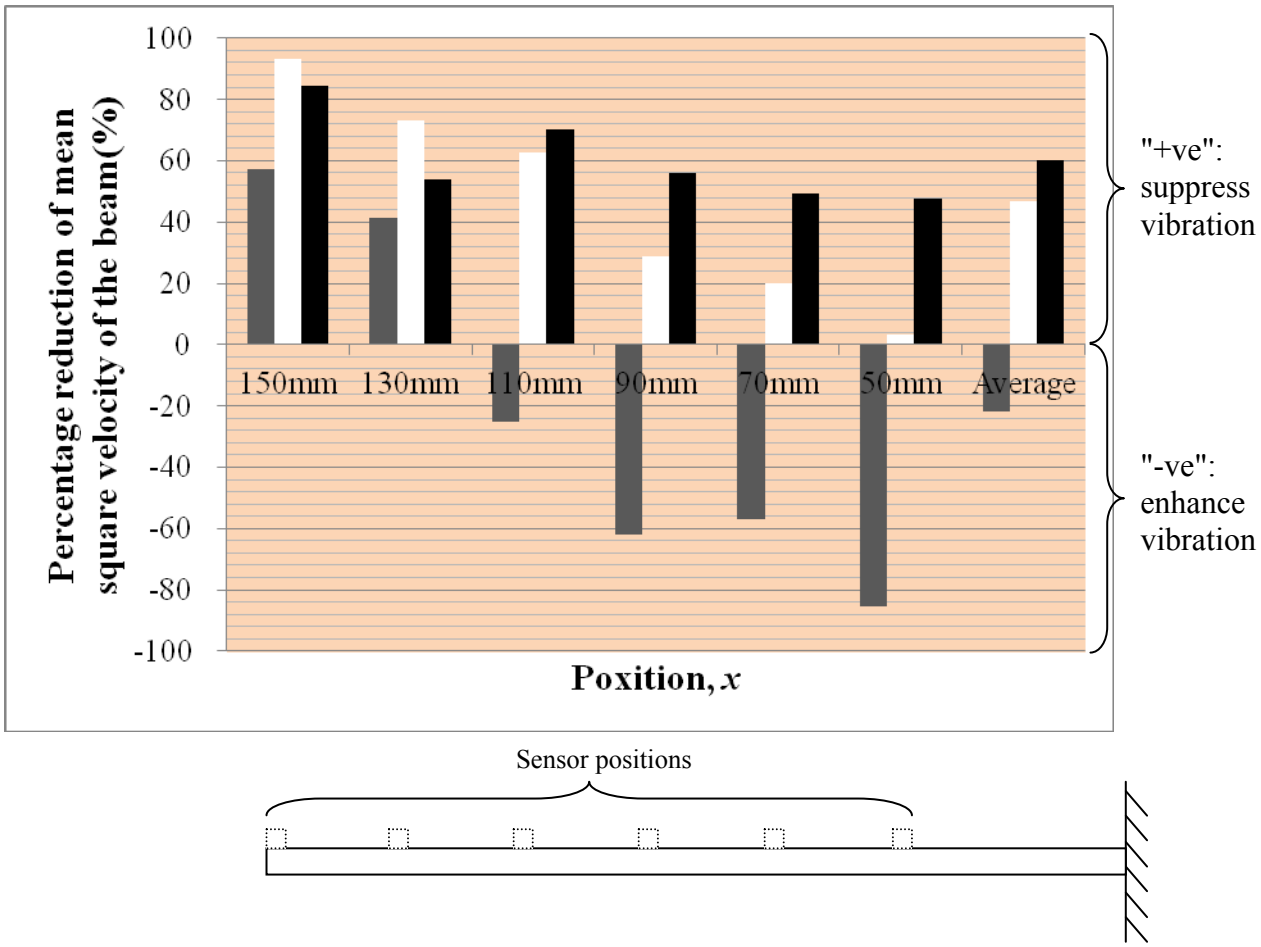

Fig. 14 Comparison of the percentage reduction of mean square velocity of the beam structure measured at x = 150mm, 130mm, 110mm, 90mm, 70mm, 50mm and the spatial average value for the cases of

(iv) passive TMD relative to raw beam, $\frac{\left(P_{x_Beam} - P_{x_TMD}\right)}{P_{x_Beam}} \times 100\%$,

(v) proposed HVA relative to raw beam, $\frac{\left(P_{x_Beam} - P_{x_HVA}\right)}{P_{x_Beam}} \times 100\%$, and

(vi) proposed HVA relative to passive TMD, $\frac{\left(P_{x_TMD} - P_{x_HVA}\right)}{P_{x_TMD}} \times 100\%$.